nature

https://doi.org/10.1038/s41586-022-05628-7

Accelerated Article Preview

Active eosinophils regulate host defense and immune responses in colitis

Received: 18 March 2022

Accepted: 6 December 2022

Accelerated Article Preview

Cite this article as: Gurtner, A. et al. Active eosinophils regulate host defense and immune responses in colitis. *Nature* https://doi.org/10.1038/s41586-022-05628-7 (2022)

Alessandra Gurtner, Costanza Borrelli, Ignacio Gonzalez-Perez, Karsten Bach, Ilhan E. Acar, Nicolás G. Núñez, Daniel Crepaz, Kristina Handler, Vivian P. Vu, Atefeh Lafzi, Kristin Stirm, Deeksha Raju, Julia Gschwend, Konrad Basler, Christoph Schneider, Emma Slack, Tomas Valenta, Burkhard Becher, Philippe Krebs, Andreas E. Moor & Isabelle C. Arnold

Active eosinophils regulate host defense and immune responses in colitis

Alessandra Gurtner[1,10], Costanza Borrelli[2,10], Ignacio Gonzalez-Perez[1], Karsten Bach[2], Ilhan E. Acar[2], Nicolás G. Núñez[1], Daniel Crepaz[1], Kristina Handler[2], Vivian P. Vu[3], Atefeh Lafzi[2], Kristin Stirm[4], Deeksha Raju[1], Julia Gschwend[5], Konrad Basler[6], Christoph Schneider[5], Emma Slack[7,8], Tomas Valenta[6,9], Burkhard Becher[1], Philippe Krebs[3], Andreas E. Moor[2,11] and Isabelle C. Arnold[1,11]

[1]Institute of Experimental Immunology, University of Zürich, Zürich, Switzerland
[2]Department of Biosystems Science and Engineering, ETH Zürich, Basel, Switzerland
[3]Institute of Pathology, University of Bern, Bern, Switzerland
[4]Institute of Molecular Cancer Research, University of Zürich, Zürich, Switzerland
[5]Institute of Physiology, University of Zürich, Zürich, Switzerland
[6]Department of Molecular Life Sciences, University of Zürich, Zürich, Switzerland
[7]Institute for Food, Nutrition and Health, D-HEST, ETH Zürich, Zürich, Switzerland
[8]Botnar Research Center for Child Health, Basel, Switzerland
[9]Institute of Molecular Genetics of the ASCR, v. v. i., Prague, 4, Czech Republic
[10]These authors contributed equally
[11]Corresponding authors: Isabelle C. Arnold, arnold@immunology.uzh.ch and Andreas E. Moor, andreas.moor@bsse.ethz.ch

In the past decade, single-cell transcriptomics has helped uncover new cell types and states and led to the construction of a cellular compendium of health and disease[1]. Still, some difficult-to-sequence cells remain absent from tissue atlases. Eosinophils, elusive granulocytes implicated in a plethora of human pathologies[2,3], are among these uncharted cell types. To date, the heterogeneity of eosinophils and the gene programs underpinning their pleiotropic functions remain poorly understood[4]. In the present study, we provide the first comprehensive single-cell transcriptomic profiling of murine eosinophils. We identify an active and a basal population of intestinal eosinophils, differing in their transcriptome, surface proteome and spatial localization. By means of a genome wide CRISPR inhibition screen and functional assays, we dissect a mechanism by which IL-33 and IFN-ɣ induce active eosinophil accumulation in the inflamed colon. Active eosinophils are endowed with bactericidal and T cell regulatory activity, and express the co-stimulatory molecules CD80 and PD-L1. Notably, active eosinophils are enriched in the

lamina propria **of a small cohort of inflammatory bowel disease patients and tightly associate with CD4$^+$ T cells. Our findings provide novel insights into the biology of this elusive cell type and highlight its crucial contribution to intestinal homeostasis, immune regulation and host defence. Furthermore, we lay a framework for the characterization of eosinophils in human gastrointestinal diseases.**

Main

Eosinophils are granulocytes that reside mainly in the thymus, uterus, lung, adipose tissue and gastrointestinal (GI) tract[1]. Their accumulation is typical of disease states such as allergic airway inflammation, atopic dermatitis, eosinophilic esophagitis and inflammatory bowel diseases (IBD)[2–5]. GI eosinophils contribute to various homeostatic processes, including epithelial barrier preservation, tissue architecture support, immune cell population maintenance as well as regulation of local immune responses[6–9]. However, their function during intestinal inflammation is unclear[10]. Moreover, the presence of functionally distinct eosinophil subsets and their ontogenetic relationship has remained unexplored due to technical challenges preventing their transcriptomic interrogation. Indeed, eosinophils are virtually absent from human and murine single cell RNA sequencing (scRNAseq) atlases[11,12], and thus represent a blindspot in our understanding of cell-type specific contributions to disease. Here, we fill this gap in knowledge by resolving eosinophil transcriptional and functional heterogeneity along their developmental trajectory from the bone marrow to tissues of residency, and by defining their role during intestinal inflammation.

A-Eos and B-Eos are two distinct GI resident eosinophil subsets

By minimising shear stress, degranulation and consequent transcript degradation (Extended Data Fig. 1a), we obtained single cell transcriptomes from eosinophils isolated from the bone

marrow (BM), blood, spleen, stomach, small intestine (SI) and colon of *Il5*-tg mice, a strain harbouring elevated eosinophil counts across tissues[13] (Extended Data Fig. 1b,c). 89% of all cells widely expressed the *bona fide* eosinophil markers *Siglecf, Il5ra, Ccr3* and *Epx* (Extended Data Fig. 1d). Clustering revealed five subpopulations ordered along a developmental trajectory (Fig. 1 a, b). Highly cycling precursors and immature eosinophils were primarily present in the BM, circulating eosinophils mainly in the blood, while two subsets, termed active (A-Eos) and basal (B-Eos), populated the gastrointestinal tissues in varying proportions (Fig. 1c, Extended Data Fig. 1e).

Eosinophil subsets exhibited distinct transcriptional profiles across organs and differed in their cytokine, effector molecule and receptor repertoire, indicating highly specialised functions (Fig. 1d, Extended Data Fig. 1f). Pseudotime analysis revealed that immature eosinophils downregulate stemness and proliferation programs, and transiently upregulate expression of granular protein (*Epx, Prg2, Ear1/2/6*) and antimicrobial peptide genes (*S100a6/9/10*) (Extended Data Fig. 1g-i). Circulating eosinophils were characterised by high expression of *Retnla* and of the adhesion protein *Cd24a*, while B-eos expressed effector molecules involved in tissue morphogenesis and remodelling such as *Mmp9* and *Tgfb1* (Fig. 1d). Placed at the end of the differentiation trajectory, A-Eos were only found in organs of the GI tract and specifically expressed genes encoding multiple bioactive factors (*Il16*, *Tnf, Il1b, Ccl3*, *Cxcl2, Vegfa, Ptgs2*) and receptors (*Il1rn, Csf2rb*, *Tgfbr2*, *Ccr1*, *Cxcr4, Ptafr, Ahr)* (Fig. 1d, Extended Data Fig. 1j). Moreover, their expression of the co-stimulatory molecules *Cd80* and *Cd274* (PD-L1) suggests A-Eos involvement in immune modulation (Fig. 1e, Extended Data Fig. 1k). We thus focused our attention on this subset.

We profiled the surface proteome of blood, SI and colon eosinophils in B6J (WT) mice by spectral flow cytometry (FACS) and found that expression of PD-L1 and CD80 was sufficient to identify A-Eos (Fig. 1f-h, Extended Data Fig 2a-c). PD-L1^{+}CD80^{+} cells expressed

A-Eos markers on the protein and RNA level (Extended Data Fig 2d-e), and exhibited higher secretory activity[14–16] (CD63, CD9, CD107a), granularity (SSC-A) and activation (Siglec F) relative to B-Eos (Fig. 1i, Extended Data Fig 2f). A-Eos further showed a peripheral distribution of eosinophil peroxidase (EPX), while granule localization in B-Eos, splenic and blood eosinophils was more cytosolic (Fig. 1j, Extended Data Fig 2g). Interestingly, A- and B-Eos differed in their spatial localization within the colonic mucosa, indicating exposure to and interactions with distinct cellular microenvironments: A-Eos were found significantly closer to the luminal extremity (luminal third), while B-Eos were retained near the submucosa (basal third) (Fig. 1k, Extended Data Fig. 2h,i). Importantly, the presence of A-Eos was restricted to the GI tract, as PD-L1^{+}CD80^{+} eosinophils were not found by FACS (Extended Data Fig 3a) nor scRNAseq (Extended Data Fig 3b-e) in other tissues of eosinophil residency such as the uterus and adipose, and only detected in small percentages in the thymus and peritoneum. A-Eos further differed from previously reported lung-resident populations and from inflammatory eosinophils recruited during house dust mite (HDM) airway challenge[17] (Extended Data Fig 3f,g).

We next wondered whether A- and B-Eos could also be found in the human GI tract, and whether their proportions are affected by colitis. We therefore subjected healthy and IBD colon tissue microarrays (TMAs) to major basic protein (MBP) and PD-L1 immunofluorescence (IF) (Extended Data Fig. 3h). Similar to our observations in mice, MBP^{+}PD-L1^{+} A-Eos were found closer to the lumen than MBP^{+}PD-L1^{-} B-Eos, indicating phenotypic correspondence (Fig. 1l). Notably, the relative abundance of A-eos (active-to-basal ratio) was 2-fold enriched in ulcerative colitis (UC) patients and 5-fold enriched in Crohn's disease (CD) specimens, relative to healthy controls (Fig. 1l). This prompted us to investigate the role of A-Eos during intestinal inflammation.

A-Eos have antibacterial and immune regulatory functions

To assess how local insults affect eosinophil subset dynamics, we evaluated the frequency of PD-L1^{+}CD80^{+} A-Eos in three distinct experimental models of GI inflammation: acute *Citrobacter rodentium (C. rod)* infection in the colon, chronic *Helicobacter pylori (H. pylori)* infection in the stomach, and dextran sulphate sodium (DSS)-induced colitis (Fig. 2a-c, Extended Data Fig. 4a). A-Eos frequencies and numbers were significantly enriched across all models, reflecting what observed in IBD and indicating that an increase in the active-to-basal ratio is a general response to epithelial damage and inflammation in the human and murine gut.

To investigate the subset-specific transcriptional changes occurring during inflammation, we profiled eosinophils from the BM, blood and colon of *C. rod*-infected and from the stomach of *H. pylori*-infected *Il5*-tg mice by scRNAseq (Extended Data Fig. 4b). We also retrieved eosinophil transcriptomes from an independent dataset of colonic MACS-enriched CD45^{+} cells of DSS-treated B6J (WT) mice[18] (Extended Data Fig. 4c). These single-cell profiles were integrated in the steady state transcriptional embedding and mapped with high confidence to the existing clusters. Of note, merging the steady state and challenge datasets did not reveal novel inflammation-specific clusters (Extended Data Fig. 4d).

Infection strongly increased the active-to-basal eosinophil ratio in the colon and stomach, and led to the accumulation of circulating eosinophils within infected tissues (Fig. 2d). Bacterial challenge further induced a relative expansion of immature eosinophils in the blood and BM. Core eosinophil populations are thus maintained during inflammation, but their proportions across organs vary in order to maximise A-Eos production at sites of infection. This compositional shift suggests alterations in the eosinophil differentiation path. Indeed, trajectory inference (Monocle[19]) and RNA velocity analysis (scvelo[20]) of BM, blood and colon eosinophils during *C. rod* infection, placed A-Eos as originating directly from immature eosinophils - rather than from B-Eos, as observed at steady state (Extended Data Fig. 4e).

Further, circulating eosinophils found in the colon, but not in the blood, of *C.rod* infected mice expressed multiple A-Eos markers, suggesting bypassing of the B-Eos maturation stage and rapid transition into the A-Eos *in situ* (Extended Data Fig. 4f). Notably, single-cell fate probabilities computed with CellRank[21] defined A-Eos as the major predicted terminal state for all eosinophil subsets, both at steady state and particularly during infection (Extended Data Fig. 4g). This suggests that B-Eos and circulating eosinophils are not alternative end states, but rather differentiation intermediates. Indeed, upon *in vitro* exposure to colon supernatant (conditioned medium, CM), eosinophils differentiated from the BM (BM-Eos, mostly precursors and immature eosinophils), or derived from blood (mainly circulating eosinophils) or spleen (mainly B-Eos) all equally acquired PD-L1^{+} and CD80^{+} surface expression in a dose-dependent manner, indicating that potential of eosinophils to differentiate into A-Eos is not restricted throughout their maturation. (Fig. 2e, Extended Data Fig. 4h). We performed genetic fate mapping in *Id2CreERT2;RosaEYPF* mice, a reporter strain in which Id2-Cre-expressing cells are inducibly labelled by EYFP. After a single tamoxifen pulse, colonic B-Eos frequencies among EYFP^{+} eosinophils decreased over time, while A-Eos frequencies increased, suggesting B-Eos to A-Eos conversion *in vivo* (Extended Data Fig. 4i). Similarly, adoptively transferred CD45.2 splenic eosinophils (B-Eos) migrated into the colon of CD45.1 hosts and showed evidence of *in situ* maturation into A-Eos (Fig. 2f). Cumulatively, these data suggest lineage plasticity and sequential ontogeny, with circulating eosinophils and B-Eos as metastable transition states along a dynamic differentiation continuum culminating with A-Eos.

To investigate the transcriptional changes elicited by infection along eosinophil maturation, we aligned BM-blood-colon trajectories during steady state and *C. rod* infection to a common pseudotime axis[22]. While at steady state the expression of genes encoding for granular proteins and antimicrobial peptides was only transiently upregulated by precursors and immature eosinophils - and therefore restricted to the BM - infection induced sustained

expression of granulogenesis and antimicrobial gene programs in circulating and colonic A-Eos (Fig. 2g, Extended Data Fig. 4j, k). Interestingly, this did not result from altered recruitment kinetics assessed by 5-ethynyl-2'-deoxyuridine (EdU) pulsing, nor from extramedullary hematopoiesis, as no lineage-committed progenitors (Il5-Ra^{+} Lin^{-} Sca-1^{-} CD34^{+}) were detected in the colon upon infection (Extended Data Fig. 4l, m). Moreover, CD63 expression in A-Eos was unaltered by bacterial challenge, indicating that the net increase in CD63 levels results from A-Eos accumulation rather than from their enhanced secretory activity (Extended Data Fig. 4n). However, colonic A-Eos exhibited a striking morphological change following *C. rod* infection, with evidence of cellular protrusions resembling extracellular DNA traps (EETs) at sites of peripheral EPX accumulation (Extended Data Fig. 4o). We previously reported impaired bacterial clearance and enhanced colonic immunopathology in *C. rod*-infected eosinophil-deficient mice[23]. Hence, we assessed the bactericidal potential of A-Eos in co-culture with a bioluminescent *C. rod* strain. Interestingly, colonic eosinophils (mainly A-Eos) as well as conditioned BM-Eos exhibited significantly greater bactericidal activity with respect to blood (circulating), spleen (B-Eos) or unconditioned BM-Eos (immature eosinophils) (Fig. 2h). Our data therefore suggest that A-Eos are a highly specialised subset involved in bacterial control and endowed with antimicrobial and cytotoxic properties.

Across all our inflammation models, A-Eos specifically upregulated gene sets involved in immune modulation, IFN-ɣ signalling and MHC-I-restricted antigen processing and presentation (Fig. 2i). Moreover, CellPhoneDB[24] identified numerous potentially interacting ligand-receptors pairs between A-Eos, CD4^{+} and CD8^{+} T cells (Extended Data Fig. 5a). Upon DSS treatment, eosinophil deficient (PHIL) mice exhibited increased colitis severity (Extended Data Fig. 5b,c) and stronger Th17 responses relative to their WT littermates, as well as elevated TNF-α and IFN-ɣ production by CD4^{+} T cells[25] (Extended Data Fig. 5d). These data

corroborate our previous report of an immune regulatory role of eosinophils[23], which, given their relative abundance and specific expression of co-stimulatory molecules, may be attributed to A-Eos. Co-culture of both conditioned and unconditioned BM-Eos with OT-I $CD8^+$ T cells, but not OT-II $CD4^+$ T cells, resulted in robust T cell proliferation in an antigen-dependent manner, suggesting that eosinophils can present antigen via MHC-I/TCR interactions (Extended Data Fig. 5e). Conversely, conditioning of BM-Eos into A-Eos was required for the downregulation of $CD4^+$ T cells proliferation following anti-CD3/CD28-mediated stimulation (Fig. 2j). Indeed, only sorted intestinal A-Eos, and not B-Eos, were able to inhibit $CD4^+$ T cell proliferation (Fig. 2k), suggesting this subset attenuates $CD4^+$ T cell responses during inflammation[9,23,26].

Of note, as IL-5 is a known driver of eosinophil maturation and survival[27], we conducted comparative flow cytometry and scRNAseq analyses between B6J and *Il5*-tg mice. Aside from higher steady state frequencies of A-Eos in *Il5*-tg mice (Extended Data Fig. 5f), we did not detect any transgene-specific effects during challenge (Extended Data Fig. 5g-i). Moreover, both subsets were similarly affected by anti-IL-5 treatment and equally depended on eotaxin/CCR3 interactions for their GI tissue accumulation (Extended Data Fig. 5j,k).

A-Eos maturation is induced locally by IL-33

Our data suggests a dual antibacterial and immunomodulatory role for A-Eos during inflammation. We next sought to acquire mechanistic understanding of the gene regulatory network governing A-Eos maturation, function and plasticity. Single-cell regulatory network inference and clustering (SCENIC[28]) revealed highly cluster-specific regulon activities and non-overlapping transcription factor profiles (Extended Data Fig. 6a, b). A-Eos exhibited high activity of several NF-κB-related regulons (Rela, Relb, Nfkb1 and Nfkb2), which were predicted to directly govern expression of *Cd274* and *Cd80* (Fig. 3a, Extended Data Fig. 6b). In line with the robust activation of this pathway indicated by both SCENIC and PROGENy

analysis (Extended Data Fig. 6c), NF-κB signalling components were specifically upregulated in A-Eos and were expressed at significantly higher levels in colonic eosinophils compared with their blood and splenic counterparts (Fig 3b, Extended Data Fig. 6d). Furthermore, the co-localization of phosphorylated NF-κB p65 (p-NF-κB p65) with $CD80^{+}$, but not $CD80^{-}$ eosinophils in the murine colonic *lamina propria* indicates selective activation of canonical NF-κB signalling in A-Eos (Fig 3c, Extended Data Fig. 6e). Notably, NF-κB inhibition *in vitro* abolished BM-Eos conditioning into A-Eos (Extended Data Fig. 6f).

Due to their proximity to the lumen, we speculated that A-Eos might be induced by microbiota-derived cues signalling via the TLR/NF-κB pathway. Indeed, the proportion of A-Eos in the colon was significantly reduced upon depletion of commensal bacteria by broad-spectrum antibiotics (Fig. 3d, Extended Data Fig. 6g) as well as in germ-free (GF) mice (Fig. 3e, Extended Data Fig. 6h). GF mice further exhibited a marked reduction in eosinophil secretory activity, most prominently in A-Eos (Extended Data Fig. 6h). However, A-Eos frequencies were not affected by TLR-2 or TLR-4 deficiency (Extended Data Fig. 6i), suggesting independence from these major bacterial recognition pathways.

To identify regulatory checkpoints of A-Eos differentiation, we conducted an *in vitro* genome wide CRISPR inhibition screen (Extended Data Fig. 7a). We found sgRNAs targeting genes involved in NF-κB and MAPK signalling to be significantly depleted in $PD\text{-}L1^{+}CD80^{+}$, but not in $PD\text{-}L1^{-}CD80^{-}$ eosinophils, compared to bone marrow stem cells (BMSCs) (Fig. 3f, Extended Data Fig. 7b). This observation is in line with our transcriptome analysis (Extended Data Fig. 1f, 6c) and suggests activation of these pathways is required for A-Eos maturation. Notably, *in vitro* stimulation with the alarmin IL-33 - but not with other cytokines such as IL-22, IL-25 and TNF-α whose levels increase during inflammation (Extended Data Fig. 7c,d) - was sufficient to induce A-Eos marker expression in a dose-dependent manner (Extended Data Fig. 7e,f). Moreover, IL-33 neutralisation significantly reduced the differentiation of

conditioned BM-Eos into A-Eos (Fig. 3g). IL-33 treatment of BM-Eos quickly led to the phosphorylation of p38 and p65, induced expression of *Cd274, Cd80* and several other A-Eos markers, and further upregulated surface presentation of its receptor ST2 (Extended Data Fig. 7g-i). *In vivo,* ST2 was expressed at higher levels by A-Eos than B-Eos, suggesting a positive feedback loop to promote tissue adaptation (Extended Data Fig. 7j). Of note, we did not detect ST2 expression in lung, adipose, uterine, peritoneal nor thymic eosinophils, further suggesting that the induction of A-Eos via IL-33 may be specific to the GI tract under homeostatic conditions (Extended Data Fig. 7k). IL-33 is known to activate the p38/MAPK and NFKB pathways via the ST2/MyD88 signalling axis[29]. Indeed, ST2-deficiency abolished the effects of IL-33 treatment in BM-Eos, and significantly reduced their ability to be conditioned by colon CM (Extended Data Fig. 7l). *In vivo*, treatment with recombinant IL-33 strikingly increased A-Eos frequencies in the colon and other organs in a MyD88-dependent manner (Fig. 3h, Extended Data Fig. 7m). Finally, A-Eos frequencies at steady state were reduced in the SI and stomach of IL-33$^{-/-}$ mice, but not in the colon, indicating that alternative, possibly microbiota-dependent mechanisms may contribute to A-Eos differentiation in the healthy colon (Extended Data Fig. 7n).

IFN-ɣ potentiates A-Eos regulatory functions during colitis

The analysis of our challenge dataset by SCENIC suggests that signalling downstream of IFN-ɣ is increased during inflammation in A-Eos. In particular, *C. rod* infection shifted the regulatory landscape towards signalling via Stats (Stat1/3/4/5b/6) and IRFs (Irf1/2/5/7/9) (Extended Data Fig. 8a). Notably, *Ifngr1* expression was restricted to the A-Eos subset (Extended Data Fig. 1j), and its deficiency in the eosinophil compartment results in decreased *C. rod* clearance and deregulated T cell responses during *H. pylori* infection[23]. To dissect the interplay of IL-33 and IFN-ɣ in regulating A-Eos functions, we performed bulk RNAseq of

BM-Eos treated with IL-33, IFN-ɣ or a combination thereof (Extended Data Fig. 8b). IL-33 induced NF-κB signalling and expression of A-Eos markers, while IFN-ɣ treatment strongly upregulated *Cd274* and genes involved in antigen presentation (Fig. 4a, Extended Data Fig. 8c). Functionally, IL-33 and IFN-ɣ treatment endowed BM-Eos with increased ability to downregulate $CD4^+$ T proliferation (Fig. 4b). Notably, the synergistic effect of IL-33 and IFN-ɣ not only increased A-Eos levels *in vitro* (Extended Data Fig. 8d), but also shifted the transcriptome of BM-Eos to a more mature state by downregulating granular protein and antimicrobial genes (Fig. 4a, Extended Data Fig. 8c). Treatment of A-Eos with IFN-ɣ further induced granule mobilisation and focal aggregation (Extended Data Fig. 8e). These results suggest a negative feedback loop on the synthesis of granular proteins and antimicrobial peptides, with their release being induced and their transcription being repressed by IFN-ɣ signalling[23,30].

In vivo, treatment with IFN-ɣ potentiated the effects of IL-33, increasing colonic A-Eos frequencies to the levels observed during colitis (Fig. 4c). Consistently, ablation of IFNGR signalling in the eosinophil compartment impaired PD-L1 upregulation in response to infection (Extended Data Fig. 8f). Notably, IFN-ɣR neutralisation abrogated *Cd274* expression but did not affect the presence of the A-Eos subset in the steady state colon, as assessed by scRNAseq (Extended Data Fig. 8g). In line with our *in vitro* results, this treatment led to the upregulation of granular protein and antimicrobial peptide genes in A-Eos (Extended Data Fig. 8g).

Our data indicate that IFN-ɣ potentiates but it is not sufficient to induce the A-Eos phenotype, which instead relies on IL-33 signalling. Indeed, IL-33-deficiency prevented the colonic accumulation of A-Eos upon DSS treatment (Fig. 4d). $IL\text{-}33^{-/-}$ mice further suffered from increased DSS-induced colitis and failed to restrict effector T cell responses (Fig. 4e,f), thus phenocopying eosinophil deficiency. Cumulatively, our data suggest that IL-33 promotes

the accumulation of A-Eos during colitis, which limit pathogen incursions and prevent excessive tissue damage through their bactericidal and T cell regulatory activities.

A-Eos co-localize with CD4$^+$ T cells in IBD patients

Finally, we performed multiplexed *in situ* RNA imaging (Molecular Cartography) in human UC colon sections (Lafzi *et al*, in preparation) and found *CD4* transcripts to be significantly co-localizing with *SIGLEC8* transcripts (Fig. 4g,h, Extended Data Fig. 8h). Indeed, 55% of *SIGLEC8*$^+$ segmented areas were also positive for *CD4* (Extended Data Fig. 8i), suggesting close spatial proximity of eosinophils and CD4$^+$ T cells in the colon of IBD patients. In a segmentation-free approach, *CD4*-neighbouring *SIGLEC8* RNA molecules were significantly more associated with the A-Eos markers *CD80, VEGFA* and *CSF2RB,* than non-*CD4*-neighbouring *SIGLEC8* molecules, indicating that CD4$^+$ T cells preferentially interact with A-Eos (Fig. 4i, Extended Data Fig. 8j). *CD4*-neighbouring *SIGLEC8* RNA molecules were also significantly associated with NF-κB (*NFKB1)* and IFN-ɣ (*IFNGR1*, *STAT1* and *IRF1)* signalling components (Fig. 4i, Extended Data Fig. 8j), suggesting that the same pathways might drive A-Eos-CD4$^+$ T cell interactions in murine and human colitis.

Discussion

Neutralising antibodies against the cytokine IL-5 are widely used in severe eosinophilic asthma to inhibit eosinophil differentiation[31]. Whether intestinal eosinophils can be exploited as therapeutic targets in IBD is still unknown, warranting a thorough investigation of their functions in the healthy and inflamed gut. Indeed, due to the technical challenges in profiling these elusive cells, eosinophils have long remained an overlooked player in colitis. Here, we identify a subset of GI-resident eosinophils enriched in IBD patients and in experimental models of colitis. In response to bacterial cues, IL-33 and IFN-ɣ signalling, A-Eos exert a

protective role on the intestinal mucosa by means of their antibacterial and immunomodulatory activity. Indeed, impaired accumulation of A-Eos in the inflamed colon worsens inflammation and leads to $CD4^+$ T cell hyperactivation during acute colitis. However, the strong effector and cytotoxic potential of this subset can potentially also favour tissue damage in settings of chronic inflammation. More studies are needed to elucidate the extent and nature of their protective activities in human intestinal homeostasis and inflammation, and whether these can be targeted for the treatment of IBD.

References

1. Marichal, T., Mesnil, C. & Bureau, F. Homeostatic Eosinophils: Characteristics and Functions. *Front. Med.* **4**, 101 (2017).
2. Blanchard, C., Wang, N. & Rothenberg, M. Eosinophilic esophagitis: Pathogenesis, genetics, and therapy. *Journal of Allergy and Clinical Immunology* vol. 118 1054–1059 Preprint at https://doi.org/10.1016/j.jaci.2006.07.038 (2006).
3. Humbles, A. A. *et al.* A critical role for eosinophils in allergic airways remodeling. *Science* **305**, 1776–1779 (2004).
4. Jenerowicz, D., Czarnecka-Operacz, M. & Silny, W. Peripheral blood eosinophilia in atopic dermatitis. *Acta Dermatovenerol Alp Pannonica Adriat* **16**, 47–52 (2007).
5. Raab, Y., Fredens, K., Gerdin, B. & Hallgren, R. *Dig. Dis. Sci.* **43**, 1061–1070 (1998).
6. Chu, V. T. *et al.* Eosinophils Promote Generation and Maintenance of Immunoglobulin-A-Expressing Plasma Cells and Contribute to Gut Immune Homeostasis. *Immunity* vol. 40 582–593 Preprint at https://doi.org/10.1016/j.immuni.2014.02.014 (2014).
7. Jung, Y. *et al.* IL-1β in eosinophil-mediated small intestinal homeostasis and IgA production. *Mucosal Immunol.* **8**, 930–942 (2015).
8. Shah, K. *et al.* Small Intestinal Resident Eosinophils Maintain Gut Homeostasis Following Microbial Colonisation. *bioRxiv* 2021.01.30.428930 (2021) doi:10.1101/2021.01.30.428930.
9. Sugawara, R. *et al.* Small intestinal eosinophils regulate Th17 cells by producing IL-1 receptor antagonist. *J. Exp. Med.* **213**, 555–567 (2016).
10. Alhmoud, T. *et al.* Outcomes of inflammatory bowel disease in patients with eosinophil-predominant colonic inflammation. *BMJ Open Gastroenterol* **7**, e000373 (2020).
11. Smillie, C. S. *et al.* Intra- and Inter-cellular Rewiring of the Human Colon during Ulcerative Colitis. *Cell* **178**, 714–730.e22 (2019).

12. Sikkema, L. *et al.* An integrated cell atlas of the human lung in health and disease. *bioRxiv* 2022.03.10.483747 (2022) doi:10.1101/2022.03.10.483747.
13. Lee, N. A. *et al.* Expression of IL-5 in thymocytes/T cells leads to the development of a massive eosinophilia, extramedullary eosinophilopoiesis, and unique histopathologies. *J. Immunol.* **158**, 1332–1344 (1997).
14. Mahmudi-Azer, S., Downey, G. P. & Moqbel, R. Translocation of the tetraspanin CD63 in association with human eosinophil mediator release. *Blood* **99**, 4039–4047 (2002).
15. Khushman, M. 'd *et al.* Exosomal markers (CD63 and CD9) expression and their prognostic significance using immunohistochemistry in patients with pancreatic ductal adenocarcinoma. *J. Gastrointest. Oncol.* **10**, 695–702 (2019).
16. Cohnen, A. *et al.* Surface CD107a/LAMP-1 protects natural killer cells from degranulation-associated damage. *Blood* **122**, 1411–1418 (2013).
17. Mesnil, C. *et al.* Lung-resident eosinophils represent a distinct regulatory eosinophil subset. *J. Clin. Invest.* **126**, 3279–3295 (2016).
18. Schwarzfischer, M. *et al.* TiO2 nanoparticles abrogate the protective effect of the Crohn's disease-associated variation within the PTPN22 gene locus. *Gut* (2022) doi:10.1136/gutjnl-2021-325911.
19. Qiu, X. *et al.* Reversed graph embedding resolves complex single-cell trajectories. *Nat. Methods* **14**, 979–982 (2017).
20. Bergen, V., Lange, M., Peidli, S., Wolf, F. A. & Theis, F. J. Generalizing RNA velocity to transient cell states through dynamical modeling. *Nat. Biotechnol.* **38**, 1408–1414 (2020).
21. Lange, M. *et al.* CellRank for directed single-cell fate mapping. *Nat. Methods* **19**, 159–170 (2022).
22. McFaline-Figueroa, J. L. *et al.* A pooled single-cell genetic screen identifies regulatory

checkpoints in the continuum of the epithelial-to-mesenchymal transition. *Nat. Genet.* **51**, 1389–1398 (2019).

23. Arnold, I. C. *et al.* Eosinophils suppress Th1 responses and restrict bacterially induced gastrointestinal inflammation. *J. Exp. Med.* **215**, 2055–2072 (2018).

24. Efremova, M., Vento-Tormo, M., Teichmann, S. A. & Vento-Tormo, R. CellPhoneDB: inferring cell–cell communication from combined expression of multi-subunit ligand–receptor complexes. *Nat. Protoc.* **15**, 1484–1506 (2020).

25. Masterson, J. C. *et al.* Eosinophil-mediated signalling attenuates inflammatory responses in experimental colitis. *Gut* **64**, 1236–1247 (2015).

26. Arnold, I. C. *et al.* The GM-CSF–IRF5 signaling axis in eosinophils promotes antitumor immunity through activation of type 1 T cell responses. *Journal of Experimental Medicine* vol. 217 Preprint at https://doi.org/10.1084/jem.20190706 (2020).

27. Griseri, T. *et al.* Granulocyte Macrophage Colony-Stimulating Factor-Activated Eosinophils Promote Interleukin-23 Driven Chronic Colitis. *Immunity* **43**, 187–199 (2015).

28. Aibar, S. *et al.* SCENIC: single-cell regulatory network inference and clustering. *Nat. Methods* **14**, 1083–1086 (2017).

29. Griesenauer, B. & Paczesny, S. The ST2/IL-33 Axis in Immune Cells during Inflammatory Diseases. *Front. Immunol.* **8**, 475 (2017).

30. Kang, K. *et al.* Interferon-γ Represses M2 Gene Expression in Human Macrophages by Disassembling Enhancers Bound by the Transcription Factor MAF. *Immunity* **47**, 235–250.e4 (2017).

31. Menzella, F. *et al.* Anti-IL5 Therapies for Severe Eosinophilic Asthma: Literature Review and Practical Insights. *Journal of Asthma and Allergy* vol. 13 301–313 Preprint at https://doi.org/10.2147/jaa.s258594 (2020).

Methods

Mice

All experiments were performed on 6-16 week-old male and female mice. C57BL/6J (B6J, stock no. 000664), and dCas9-KRAB (stock no.030000) mice were obtained from The Jackson Laboratory; OT-1 (stock no. 003831), OT-II (stock no. 004194), MyD88$^{-/-}$ [32], Tlr2$^{-/-}$ (stock no. 004650), CD45.1 (stock no. 002014), Tlr4$^{-/-}$ [33] mice were obtained from a local live mouse repository. Id2^{CreERT2};Rosa26^{EYFP} mice[34], *Il5*–transgenic mice[35] and Ifngr2$^{fl/fl}$ mice[36] have been previously described. Il33$^{-/-}$ [37] were obtained through the RIKEN Center for Developmental Biology (Acc.No.CDB0631K) and St2$^{-/-}$[38] mice have been described and backcrossed onto a C57BL/6J background. Eosinophil-deficient mice[39] (PHIL) and mice expressing Cre under the EPX promoter[40] (Eo-*Cre*) were obtained from J.J. Lee (Mayo Clinic, Phoenix, AZ). Chow and water were available *ad libitum*, unless specified. All mice were in the B6J background and maintained on a 12h light / 12h darkness schedule. Mice were housed and bred under specific pathogen-free conditions in accredited animal facilities. Germ-free mice were bred and maintained in open-top cages within flexible-film isolators, supplied with HEPA-filtered air, and autoclaved food and water *ad libitum*. At the experimental endpoint, mice were sacrificed by raising CO_2 concentrations. All experimental procedures at the University of Zurich and Bern were performed in accordance with Swiss Federal regulations and approved by the Cantonal Veterinary Office and/or in accordance with the European Communities Council Directive (86/609/EEC), Czech national guidelines, institutional guidelines of the Institute of Molecular Genetics and approved by the Animal Care Committee.

Animal experiments

Antibody neutralisation: 10 days treatment: 7-8 week-old females and males (B6J) were injected intraperitoneally (i.p.) twice per week with 0.5mg anti-IL-5 (BE0198 BioXCell, TREK5) or anti keyhole limpet hemocyanin isotype control (BE0090, BioXCell, LTF-2), or anti-IFN-ɣR (BE0029, BioXCell, GR-20) or anti-CCR3 (BE0316 clone 6S2-19-49) or anti-horseradish peroxidase isotype control (BE0088, BioXCell, HRPN) antibodies for 10 days before the study endpoint.

Intestinal commensal depletion by antibiotic treatment: 7-8 week-old females (B6J) were treated for 10 consecutive days with ampicillin (1g/L; A0166 Sigma), vancomycin (500mg/L; A1839,0001 Applichem), neomycin sulphate (1g/L; 4801 Applichem), and metronidazole (1g/L; H60258 Alfa Aesar) in autoclaved drinking water, as previously described[41]. Water bottles were monitored and refilled twice per week.

Adoptive transfer: 10^6 cells magnetically-selected splenic eosinophils of 6-12 week-old *Il5*-tg females and males were injected intravenously in 100µL PBS into CD45.1 recipients (8-12 week-old female and male mice). Organs were harvested 42 hours after injection.

DSS-induced colitis: 6-12 week-old females and males (PHIL, B6J and Il33$^{-/-}$) were treated with 2.5% Dextran Sulphate Sodium (DSS) (wt/vol; 9011-18-1, MP Biomedicals) dissolved in autoclaved drinking water for 5 days, followed by 3 days of regular water, before organ harvesting. Water bottles were monitored and refilled twice per week.

Bacterial challenge infection, H. pylori: 6-12 week-old females and males (*Il5*-tg and B6J) were infected orally with *H. pylori* strain PMSS1 (10^7 colony-forming units, CFU) and

analysed 4 weeks post-infection. The PMSS1 strain, a clinical isolate of a duodenal ulcer patient, was grown on horse blood agar plates followed by liquid culture, as previously described[27]. Cultures were routinely assessed by light microscopy for contamination, morphology and motility. *C. rodentium:* 6-12 week-old females and males (*Il5*-tg and B6J) were infected orally with the nalidixic acid-resistant *C. rod* strain ICC169 (ATCC 51549, 10^8 CFU) and analysed 13 days post-infection. Bioluminescent *C. rodentium* strains ICC180 (ICC169 derivative, nalidixic acid- and kanamycin-resistant) was a kind gift of Gad M. Frankel, Imperial College London, UK and was previously described[42]. Both strains were grown on agar plates (1.5%; A0927 Applichem), followed by single-colony picking and overnight culture in antibiotic-supplemented Luria broth (nalidixic acid, 50 μg/mL; N4382 Sigma and/or kanamycin, 50 μg/mL; 420311 Sigma).

Cytokine administration: 7-8 week-old females ($MyD88^{-/-}$ and B6J) were injected intraperitoneally (i.p.) every other day with three total doses of 0.5mg recIL-33 (210-33, PeproTech) and/or IFN-ɣ (315-05, PeproTech) or with PBS control.

EdU labelling: 7-8 week-old females and males (*Il5*-tg and B6J) were infected orally with *C.rod* or left uninfected; 4 days prior to analysis mice were injected with EdU (2.5mg/ mouse, 900584 Sigma).

HDM challenge: 4 month-old females (B6J) received 1μg HDM extract in 50μL PBS intratracheally for sensitization (day 0) and were then challenged once a day with 10μg HDM in 50μL PBS for 5 days (day 7-11). Lungs were harvested 14 days after the sensitization.

Tamoxifen injection: 6-12 week-old females and males ($Id2^{CreERT2}$;$Rosa26^{EYFP}$) were gavaged with a single dose of tamoxifen (T5648 Sigma). Tamoxifen was dissolved in a small volume of 100% ethanol (pre-warmed at 50°C) and then resuspended in corn oil (pre-warmed at 50°C) to the final concentration of 5mg / mouse. Organs were harvested 2 hours, 2 and 4 days after the injection.

Preparation of single-cell suspensions from tissues

Gastrointestinal tissues: stomach, colon and small intestine (SI) were harvested, cleaned of faecal matter and cut longitudinally. Organs were washed in PSB and cut into pieces (1-2cm) and Peyer's patches were removed from the SI. Pieces were washed twice in a shaking incubator with wash buffer (2% BSA, 100 U/mL penicillin/streptomycin, 5 mM EDTA in HBSS, 25 minutes, 37 °C). Tissues were then rinsed in cold PBS and digested for 50 minutes at 37°C in complete medium (10% FBS, 100 U/mL, penicillin/streptomycin (P0781 Sigma) in RPMI-1640) containing 15 mM Hepes (H0887 Sigma), 0.05 mg/mL DNase I (10104159001 Roche) and an equal amount of 250 U/mL type IV (C5138 Sigma) and type VIII collagenase (C2139 Sigma) (for colon and SI), or 500 U/mL type IV collagenase (C5138 Sigma) (for stomach). Cells were passed through a 70μm cell strainer, centrifuged for 8 minutes and layered onto a 40/80% Percoll (17089101 Cytiva) gradient (18 minutes, 2100 g, 20°C, no brake). The interphase was collected and washed in PBS.

Lung: lungs were perfused with PBS, harvested and cut into pieces before digestion in complete medium supplemented with 500 U/mL type IV collagenase (Sigma) and 0.05 mg/mL DNase I (Roche) for 50 minutes at 37°C. Lungs were then passed through a 70μm cell strainer and mesh with syringe plungers. To reduce macrophage contamination (Siglec F^+), cells were plated in complete RPMI medium for 1 hour at 37°C.

Blood: blood was sampled by post-mortem cardiac puncture in 2% BSA 5mM EDTA PBS. For *Il5*–tg mice, the suspension was layered over Histopaque 1119 (density of 1.119 g/mL; 11191 Sigma-Aldrich) and centrifuged at 800g for 20 minutes and the interphase was washed in PBS. Red blood cells were lysed in ice-cold distilled water for 30 seconds.

Bone marrow (BM): femur and tibia were flushed using complete RPMI medium and a 23-gauge needle. The content was collected, filtered through a 40µm cell strainer and red blood cells were lysed in ice-cold distilled water for 30 seconds.

Spleen, lymph nodes and thymus: spleen and lymph nodes were harvested, meshed through a 40µm cell strainer using a syringe plunger, and red blood cells were lysed in ice-cold distilled water for 30 seconds.

Peritoneal fluid: peritoneal cavity was perfused with 5 mL PBS with a 21-gauge needle and the inflated area was massaged for 30 seconds, to disperse the solution. The peritoneal liquid was collected and cells were plated in complete RPMI medium for 1 hour at 37°C to remove adherent cells.

Adipose tissue: lungs were perfused with PBS and the perigonadal adipose depot was isolated, removing any visible gonadal tissue. The tissue was minced into small pieces and digested in complete DMEM medium supplemented with 0.2mg/mL Liberase (05401020001 Roche) and 0.05 mg/mL DNase I (Roche) for 50 minutes at 37°C. Suspensions were filtered through a 100µm cell strainer and centrifuged at 1000g for 10 minutes. The pellet was collected and washed in PBS.

Uterus: uterus was harvested, cut longitudinally and washed in PSB. Pieces were shaken in wash buffer (2% BSA, 100 U/mL penicillin/streptomycin, 5 mM EDTA in HBSS, 25 minutes, 37 °C). The tissue was then rinsed in cold PBS and digested for 50 minutes at 37°C in complete medium containing 0.05 mg/mL DNase I (Roche) and 0.2mg/mL Liberase (Roche). Cells were passed through a 70µm cell strainer, centrifuged and washed in PBS.

Unless specified, all centrifugation steps were performed at 500 g for 8 minutes at 10°C.

Magnetic cell enrichment

Eosinophils of 6-12 week-old females and males (*Il5*-tg) were positively-enriched using a PE anti-mouse Siglec F antibody (562068 BD Biosciences; E50-2440) and anti-PE microbeads (130-042-401 Miltenyi Biotech), according to the manufacturer's instructions. Immune cells of 7-8 week-old females (B6J) were positively-enriched using anti-CD45 microbeads (130-052-301 Miltenyi Biotech), according to the manufacturer's instructions.

Single-cell RNA sequencing

Single cell capture and library preparation: Whole transcriptome analyses of magnetically-enriched Siglec F^+ eosinophils (blood, spleen, stomach, colon, SI, adipose tissue, lung and uterus, *Il5*-tg), total bone marrow cells (*Il5*-tg) or $CD4^+$ cells (colon, B6J) were performed using the BD Rhapsody Single-Cell Analysis System (BD, Biosciences). Cells were pooled from 3-5 mice per sample. Tissue processing and enrichment procedures are described above. Each preparation was assessed by flow-cytometry to determine eosinophil viability and was subjected to morphological examination upon cytospin and staining. Eosinophils were labelled with sample tags (633793 BD Mouse Single-Cell Multiplexing Kit) according to the manufacturer's protocol. Briefly, for each condition, 10^6 cells were resuspended in staining

buffer (1% BSA, 1% EDTA in PBS) and incubated with the respective Sample Tag for 20 minutes at room temperature. Cells were then transferred to a 5 mL polystyrene tube, washed two times with 2 mL staining buffer and centrifuged at 400g for 5 minutes. Samples were resuspended in 1 mL staining buffer for counting. 10'000 or 20'000 cells from up to 4 barcoded samples were pooled for a total of 60'000 cells, the mixture was centrifuged at 400g for 5 minutes. The pellet was resuspended in 650 BD Sample Buffer supplemented with 1:1000 SUPERase in (20U/µL; AM2694 ThermoFisher) and NxGen Rnase Inhibitor (40U/µL; 30281-2 Lucigen). BD Rhapsody cartridges were super-loaded with 60'000 cells each. Single cells were isolated with the BD Rhapsody Express Single-Cell Analysis System according to the manufacturer's recommendations (BD Biosciences). cDNA libraries were prepared using the BD Rhapsody Whole Transcriptome Analysis Amplification Kit (633801 BD Biosciences) following the BD Rhapsody System mRNA Whole Transcriptome Analysis (WTA) and Sample Tag Library Preparation Protocol (BD Biosciences). The final libraries were quantified using a Qubit Fluorometer with the Qubit dsDNA HS Kit (Q32851 ThermoFisher). Library size-distribution was measured with the Agilent high sensitivity D5000 assay on a TapeStation 4200 system (5067-5592 Agilent technologies). Sequencing was performed in paired-end mode (2*75 cycles) on a NovaSeq 6000 with NovaSeq 6000 SP Reagent Kit chemistry.

Data pre-processing and normalisation: After demultiplexing of bcl files with Bcl2fastq v2.20.0.422 (Illumina) and quality control, paired-end scRNAseq FASTQ files were processed on the Seven Bridges Genomics platform with default parameters. Downstream analysis was conducted in *R* version 4.1.0 with package *Seurat* version 4.0.3[43]. All Seurat objects (one for each of the multiplexed samples) were merged and subjected to the same quality filtering. Cells with < 200 or > 2.500 detected genes were excluded from the analysis. After LogNormalization, the count data was scaled regressing for mitochondrial reads, and principal component analysis (PCA) was performed based on the 2,000 most variable features. Clustering and UMAP visualisation were performed on the merged dataset using 50 principal components and a resolution of 0.3 for the shared nearest neighbour clustering algorithm. The clusters were annotated manually based on marker gene expression. Epithelial and mesenchymal contaminants, as well as immune cell clusters not belonging to the eosinophil-lineage were excluded from downstream analysis. A cluster high in mitochondrial genes was excluded as well. The eosinophil space was analysed by subsetting clusters expressing eosinophil markers. The subsetted dataset was subjected to normalisation, scaling and to PCA as above. Clustering and UMAP visualisation was performed using 20 principal components and a resolution of 0.3 for the shared nearest neighbour clustering algorithm. For the lung, uterus and adipose tissue dataset, batch correction was performed with harmony[44] and epithelial genes (markers genes of epithelial cluster with pct.2 < 0.05) derived from excessive cell free RNA were removed from the counts.

Differential gene expression analysis, gene set enrichment and score computation: To extract cluster markers, *FindAllMarkers* was executed with *logfc.threshold* and *min.pct* cutoffs set to 0.25. Top-ranked genes (by logFC) were extracted for illustration. For differential gene expression, *FindMarkers* was applied with *logfc.threshold* and*min.pct* set to 0. Genes were subsequently filtered based on Bonferroni-adjusted p-value < 0.05. Scores were computed with the *AddModuleScore* function. Genes used for the scores and signatures were manually curated from GO terms and literature, and are listed in Table S3. Cell cycle scoring was performed with

the CellCycleScoring algorithm from Seurat, using cell cycle-related genes from[45]. For Gene Set Enrichment Analysis (GSEA), differentially expressed genes were pre-ranked in decreasing order by the negative logarithm of their p-value, multiplied for the sign of their average log fold change (in R, '- *log(p_val)*sign(avg_log2FC)*'). GSEA was performed on this pre-ranked list using the R package *FGSEA* (https://github.com/ctlab/fgsea/) with default parameters and the Gene Ontology Biological Process database, made accessible in R by the package *msigdbr*, https://github.com/cran/msigdbr). The results were filtered for significantly enriched gene sets (Bonferroni-adjusted p-value < 0.05).

Trajectory inference and trajectory alignment: Trajectory inference was performed with Monocle 2.3.6[19,46] in R version 3.6.3. After creating a Monocle object using "negbinomial.size()" distribution and lowerDetectionLimit = 0.5, the analysis was performed using Seurat's top 2000 variable features as ordering genes. Dimensionality reduction was performed using the "DDTree" method. To visualise the eosinophil differentiation, cluster annotations were projected on the inferred trajectories. Trajectory alignment of the bone marrow-blood-colon trajectories was performed by applying dynamic time warping as performed by[22,47]. The steady state and *C. rodentium*-challenge trajectories were set as the reference and query, respectively. Differentially expressed genes were identifying by using a full model of '*y ~ pseudotime*treatment*' and a reduced model of '*y ~ pseudotime'*.

RNA velocity and cell fate probabilities: Loom files were generated with velocyto[48] and dynamical velocities were computed with scvelo[20]. Fate probabilities were computed with CellRank[21] and plotted as pie charts (partition-based graph abstraction, PAGA).

Pathway and regulon activity analysis: Pathway activity was calculated across eosinophil subsets with PROGENy version 1.13.2[49] with default parameters. Gene regulatory activity was interrogated by applying SCENIC 1.2.4[28] with default parameters. Briefly, after expression matrix filtering (*minCountsPerGene = 3*.01*ncol(exprMat), minSamples = ncol(exprMat)*.01*), and computing correlation, GENIE3 was applied to infer potential transcription factor targets. Coexpression networks were then calculated, regulons were created and their activity was scored in cells. Regulon activities were visualized as cluster averages using the R package ComplexHeatmap[50].

Integration of datasets: Challenge, DSS and B6J datasets were integrated using Seurat's anchoring-based integration method using the steady state object as reference dataset (*reference.reduction = "pca", dims = 1:50*).

Cell-cell interaction prediction with CellPhoneDB: Ligand-receptor interaction analysis was performed using the python package CellPhoneDB (version 2.0.0, python version 3.8.5) following instructions from the GitHub repository (https://github.com/Teichlab/cellphonedb). In brief, the annotated Seurat object of isolated LP immune cells from DSS-treated B6J mice was used to test expression of known ligand-receptor interactions from the public repository of CellPhoneDB. Gene symbols were first converted from mouse to human using the biomart R package (version 2.46.3). Mean values representing the average ligand and receptor expression of annotated clusters were calculated based on the percentage of cells expressing the gene, and the gene expression mean. To determine significance of observed means, p-values were calculated using a null distribution of means calculated for randomly permuted annotated cluster labels. An interaction was considered significant if p-values ≤ 0.05. Significant ligand receptor interaction pairs between eosinophils and $CD8^+$ T cells or $CD4^+$ T cells were extracted,

gene symbols were converted from human to mouse, and their mean values were plotted using the plot_cpdb function from the ktplots R package (version 1.1.14) (https://github.com/zktuong/ktplots).

Plotting and statistical analysis: Statistical analysis and visualization were performed using R version 3.6.3 or 4.1.0. Statistical significance tests were performed as described in each figure legend. Unless stated otherwise all tests were significant with Bonferroni-adjusted p value < 0.05. Plots were generated with the R package ggplot2[51].

Flow cytometry, cell sorting and counting

Staining: For surface staining, cells were stained in PBS at 4°C for 30 minutes with the fixable viability dye eFluor 780 (1:1000, 65-0865-14 eBioscience) and a combination of the following antibodies (1:200, all from BioLegend; unless stated otherwise): anti-mouse CD45 BV650 (30-F11, 103151), CD11b BV510 (M1/70, 101263), MHC-II AF700 (M5/114.15.2, 107622), Ly6G Percp-Cy5.5 (1A8, 127616), CD4 PerCP (RM4-5, 100538), TCRβ PE-Cy7 (H57-597, 109222), TCRβ PE-Cy7 (H57-597, 109228), CD80 BV605 (1:100, 16-10A1, 104729), PD-L1 PE-Cy7 (1:100, 10F.9G2, 124314), CD31 PE (390, 102408), CD45.2 BV785 (1:50, 104, 109839), CD9 PE (MZ3, 124805), CD54 BV711 (YN1/1.7.4, 116143), CD63 PE (1:100, NVG-2, 143904), CD95 PE-Cy7(SA367H8, 152607), SiglecE PE (M1304A01, 677104), Sca-1 AF488 (D7, 108116), Sca-1 AF700 (D7, 108142), C-kit BV605 (ACK2, 135121), CD11c APC-Cy7 (N418, 117323), Clec12a PE (5D3, 143404), CD49d FITC (R1-2, 103605), CD16/32 FITC (S17012B, 101305), CD3e Percp-Cy5.5 (145-2C11, 100328), CD8a APC (53-6.7, 100712), NK1.1 Percp-Cy5.5 (PK136, 108727), B220 Percp-Cy5.5 (RA3-6B2, 103236), Ter119 Percp (TER-119, 116227), Gr1 Percp (RB6-8C5, 108427), CD34 AF647 (RAM34, 560230), Siglec F BV421 (E50-2440, 552681 BD Biosciences), Siglec F PE (E50-2440, 552126 BD Biosciences), CD125 PE (T21, 558488 BD Biosciences), CD275 (HK5.3, 50598582 eBioscience), T1/ST2 FITC (1:100, DJ8, 101001F MD Bioproductos GmbH). For T cell intracellular cytokine staining, cells were incubated for 3.15 hours in complete IMDM medium containing 0.1 μM phorbol 12-myristate 13-acetate (P-8139 Sigma) and 1 μM ionomycin (I-0634 Sigma) with 1:1000 Brefeldin A (00-4506-51 eBioscience) and GolgiStop solutions (51-2092KZ BD Biosciences) in a humidified incubator with 5% CO_2 at 37°C. Following surface staining, cells were fixed and permeabilized with the Cytofix/Cytoperm Fixation/Permeabilization Solution kit (512090KZ BD Biosciences) according to the manufacturer's instructions. Cells were then stained for 50 minutes with anti-mouse IL-17A APC (TC11-18H10.1, 506916), IFN-ɣ BV421 (XMG1.2, 505830) and TNF-α FITC (MP6-XT22, 506 304) all from Biolegend at 1:100. Fc block (anti-CD16/CD32, 101302 Affymetrix) was included to minimise nonspecific antibody binding. Total leukocyte counts were determined by adding countBright Absolute Counting Beads (C36950 Life Technologies) to each sample before analysis. Samples were acquired in a LSRII Fortessa or FACS AriaIII 5L (BD Biosciences). For high-dimensional spectral flow-cytometry analysis, cells were acquired on Cytek Aurora 5L (Cytek Biosciences) following 50 minutes staining at 4°C with the antibodies described in Table S5. For Click-iT Plus EdU Alexa Fluor 647 Flow Cytometry Assay Kit (C10419 ThermoScientific), the staining protocol was followed according to manufacturer's instructions. BD FACSDiva Software (BD Biosciences) was used for data acquisition and cell sorting.

Data analysis and plotting: Flow cytometry data analysis was performed with FlowJo software (version 10.7.1 Becton Dickinson & Company). Cell counts, relative cell frequencies or mean fluorescence intensity (MFI) were used to generate graphical plots in GraphPad Prism (version 9.1.1, GraphPad). High dimensional flow cytometry data were compensated and exported with FlowJo software (version 10) and the resulting FCS files were uploaded into Rstudio (version 4.0.3 R software environment). UMAPs were generated on stochastically selected cells from each sample and FlowSOM metaclusterings were performed for all the exported events as described previously[52].

Statistical analysis: All statistical analyses were performed with GraphPad Prism (version 9.1.1, GraphPad). Two-tailed unpaired Student's *t*-test was used for comparing two groups, while comparisons of more than two datasets was done using one-way analysis of variance (ANOVA) with Tukey's post-test. Differences were considered statistically significant when $P < 0.05$.

Isolation and culture of mouse BM-derived eosinophils

To generate murine BM-derived eosinophils (BM eos), BM cell suspensions were seeded at a density of 10^6 cells/mL in RPMI-1640 medium supplemented with 20% heat inactivated FBS, 25 mM Hepes (H0887 Sigma), 100 U mL−1 penicillin/streptomycin (P0781 Sigma), 2 mM glutamine (25030-024 Gibco), 1xNEAA (11140-035 Gibco), and 1 mM sodium pyruvate (11360070 Gibco). Cells were cultured in a humidified incubator with 5% CO_2, 37°C, and were supplemented with 100 ng/mL mouse SCF (250-03 PeproTech) and 100 ng/mL mouse FLT3-Ligand (250-31L PeproTech) from day 0 to day 4, followed by differentiation with 10ng/mL murine rec-IL-5 (215-15 PreproTech) until day 13, as described[53]. Half of the medium was replaced and the cell concentration was adjusted to 10^6 cells/mL every other day. On day 8, cells were collected and moved to new flasks to remove adherent contaminating cells. On day 13, the nonadherent cells were collected and washed with PBS. Eosinophils were sorted and purity was assessed by flow cytometry (>95%).

In vitro conditioning with supernatant of cultured colonic explants and cytokines

Supernatant of cultured colonic explants (colon CM) was prepared by culturing mid colon sections (~0.3 cm) from 6-12 week-old females and males (B6J) in 300µL of complete RPMI medium in a humidified incubator with 5% CO_2, 24 hours at 37°C. Flow-cytometry-purified eosinophils were magnetically isolated from blood and spleen (*Il5*-tg) or differentiated from the BM (B6J) and were kept in complete RPMI medium with recombinant murine IL-5 (10ng/mL, PreproTech). Cells were seeded in round-bottom 96-well plates at a density of $2x10^5$ cells / well (100µL) and conditioned for 12 hours at 37°C with cell-free colon CM (1:10 or at the indicated doses) or the following cytokines: IL-22 (10ng/mL, 210-22 PreproTech), IL-25 (10ng/mL, 210-17E PreproTech), TNF-α (10ng/mL, 315-01A PreproTech) and IL-33 (20ng/mL or at the indicated doses, PeproTech). The NF-κB inhibitor BAY11-7082 (B5556, Sigma) was added at a concentration of 5 uM and anti-IL-33 neutralising antibody (AF3626, Biotechne) at 30ng/mL. To study granule mobilisation, magnetically-enriched splenic eosinophils (*Il5*-tg) were treated overnight with colon CM (1:10) and flow-cytometry sorted A-Eos were conditioned with IFN-ɣ (20ng/mL, PeproTech) for 90 minutes.

C. rodentium ICC180 viability assay

Flow-cytometry-purified BM-Eos (B6J) or magnetically-enriched colonic, splenic and blood eosinophils (*Il5*-tg) from 6-12 week-old females and males were used for the assay. BM-Eos were conditioned overnight with colon CM (1:10) at 37°C. Eosinophils were washed with PBS and transferred to a white flat-bottom 96-well plate (Corning) in antibiotic-free RPMI-1640 medium supplemented with 10% FBS and murine IL-5 (10 ng/mL, PeproTech). 10^8 bioluminescent *C. rod* bacteria (at exponential phase, 1–1.5 OD600) were added to each well and luminescence was measured after 60 minutes on an Infinite 200 PRO plate reader (TECAN).

T cell proliferation assay

Flow-cytometry-purified BM-Eos (B6J) or magnetically-enriched splenic eosinophils (*Il5*-tg) or A-Eos and B-Eos sorted from the GI tract (*Il5*-tg) were isolated from 6-12 week-old females and males. BM-Eos or spleen-derived eosinophils were conditioned overnight with colon CM (1:10) or treated with recombinant mouse IFN-ɣ (10ng/mL, PeproTech) and/or IL-33 (20ng/mL, PeproTech), as indicated. Naïve $CD4^+$ T cells were isolated from the lymph nodes of 6-12 week-old females and males (B6J), enriched with the MojoSort Mouse CD4 Naïve T Cell Isolation Kit (480040 BioLegend) and purified by flow-cytometry. T cells were labelled with the CellTrace CFSE Cell Proliferation Kit (C34554 ThermoFisher) following manufacturer's instructions. T cells were then activated by CD3/CD28 T-activator Dynabeads (11131D Gibco) and co-cultured with eosinophils at a 1:1 ratio ($2x10^5$ total) for 4 days at 37°C in complete RPMI medium supplemented with 10 ng/mL recombinant mouse IL-5 (PeproTech) and 20 ng/mL IL-2 (402-ML R&D). CFSE dilution was assessed by flow cytometry.

Antigen presentation assay

BM-Eos were isolated from 6-8 week-old females and males (B6J) and purified via flow cytometry. Eosinophils were conditioned overnight with colon CM, where indicated. Cells were washed in PBS and loaded with 300 ng/mL of ovalbumin (OVA) residues 257-264 (S7951 Sigma) or 323-339 (O1641 Sigma) for 6 hours in complete RPMI medium supplemented with 10 ng/mL recombinant IL-5 (PeproTech). T cells were sorted by flow-cytometry and labelled with CellTrace CFSE Cell Proliferation Kit (C34554 ThermoFisher) following manufacturer's instructions. OT-I $CD8^+$ and OT-II $CD4^+$ T cells were obtained from the lymph nodes of 8-12 week-old females and males (OT-I and OT-II, respectively). T cells were co-cultured with eosinophils at a 1:1 ratio ($2x10^5$ total) for 4 days at 37°C in complete RPMI medium supplemented with 10 ng/mL recombinant mouse IL-5 (PeproTech) and 20 ng/mL IL-2 (402-ML R&D). CFSE dilution was assessed by flow cytometry.

Quantitative RT-PCR

The RNA cultured BM-Eos (B6J) or A-Eos and B-Eos sorted from the SI (*Il5*-tg) was isolated using Direct-zol RNA MicroPrep kit (R2062 Zymo Research), while the RNA from magnetically-enriched colonic, splenic and blood eosinophils from 6-12 week-old females and males (*Il5*-tg) was isolated using RNeasy Mini kit (74106 QIAGEN). Both isolations were performed according to the manufacturer's instructions, including on-column DNase 1 digestion step. Complementary DNA synthesis was performed using Superscript III reverse

transcription (18080-044 QIAGEN). Gene expression was measured on a CFX384 Touch Real-Time PCR system (BioRad, Second Derivative Maximum method analysis with high confidence algorithm) by TaqMan Gene Expression Assays (4331182 Applied Biosystems by ThermoFisher Scientific): *Cxcl2* (Mm00436450_m1), *Hprt* (Mm03024075_m1), *Gapdh (Mm99999915_g1), Cd274* (Mm03048248_m1), *Cd80 (Mm00711660_m1), Ahr (Mm00478932_m1), Nfkb1 (Mm00476361_m1), Nfkb2 (Mm00479807_m1), Rela (Mm00501346_m1), Tnfa (Mm00443258_m1), Il1b (Mm00434228_m1), Ptgs2 (Mm00478374_m1).* Gene expression levels for each sample were normalized to *Hprt* or *Gapdh* expression. Mean relative gene expression was determined, and the differences calculated using the 2ΔC(t) method.

Bulk RNA sequencing

BM-Eos were isolated from 7-8 weeks old females and males (B6J) , differentiated and flow-cytometry-purified. Cells were plated at the density of $5x10^5$ cells / well (250µL) and conditioned overnight with recombinant IL-33 (20ng/mL PeproTech) and/ or IFN-ɣ (15ng/mL PeproTech). RNA isolation was performed with RNeasy Mini kit (74106 QIAGEN) according to the manufacturer's instructions, including on-column DNase 1 digestion step. RNA quality was assessed by Tapestation (Agilent). Library preparation was performed with the Illumina TruSeq RNA Kit. RNA sequencing was performed on the Illumina Novaseq 6000 (200 Mio reads), single end read 100bp. Reads were quality-checked with FastQC. Reads alignment to the reference genome "Mus_musculus.GRCm39" and read count was performed on the Support Users for SHell script Integration (SUSHI) framework[54], with the RSEMApp application. Filtering and differential expression testing were performed with edgeR[55]. The package pheatmap[56] was used to generate heatmaps.

Immunofluorescence

Mouse colonic sections: the colon of 7-8 week-old females and males (B6J) was dissected out, flushed in PBS and fixed 3 hours in PFA (4% in PBS) at 4 °C, followed by overnight incubation in sucrose (30% w/v in 4% PFA) at 4 °C. Tissue was embedded in Tissue-Tek OCT Compound (Sakura, 4583) and stored at -80 °C. Tissue from 3-4 mice was cryosectioned (8µm) onto the same microscope slide, washed in PBS and incubated for 1 hour in blocking solution (2.5% BSA, 5% heat-inactivated normal goat serum, 0.1% Tween-20 in PBS) at room temperature. Slides were incubated overnight in blocking solution with the following primary antibodies (1:100): rat anti-mouse SiglecF (E50-2440, 552126 BD Biosciences), Armenian hamster anti-mouse CD80 (16-10A1, 104729 Biolegend) and rabbit anti-mouse p-NF-κB p65 (Ser536) (93H1,3033S Cell Signalling). After washing 3x with PBST (0.1% Tween in PBS), the following secondary antibodies were added (1:400 in blocking solution) to the slides for 1 hour at RT: AlexaFluor goat anti-rat 594 (A-11007), AlexaFluor goat-anti hamster 647 (A-21451), AlexaFluor goat anti-rabbit 488 (A-11008) all from ThermoFisher. Slides were washed 4x 5 minutes with PBST, and DAPI (D9542 Sigma, 1:1000) was added to the third washing step. Slides were mounted in Prolog Gold (P36930 Invitrogen) and imaged on a Nikon Ti2-E inverted microscope, equipped with CrestOptics X-Light v3 confocal disk unit, Lumencor Celesta lasers and Photometrics Kinetix camera.

Human tissue microarrays: the microarrays CO245 and CO246 were obtained from Biomax.us. Deparaffinized sections were subjected to antigen retrieval in 2.4 mM sodium citrate and 1.6 mM citric acid, pH 6, for 25 minutes in a steamer. Sections were washed with PBST and blocked for 1 hour at RT in blocking buffer (5% BSA, 5% heat-inactivated normal goat serum in PBST). Slides were incubated overnight at 4 °C with the following primary antibodies (1:100, in blocking buffer): mouse anti-human MBP (BMK-13, anti-human MBP (BMK-13, MCA5751 Bio-RAD), rabbit anti-human PD-L1 (E1L3N, 13684S Cell Signalling). After washing 3x with PBST (0.1% Tween in PBS), the following secondary antibodies were added (1:400 in blocking solution) to the slides for 1 hour at RT: AlexaFluor goat anti-rabbit 594, AlexaFluor goat-anti mouse 647 (ThermoFisher). DAPI staining, mounting and imaging were performed as above.

Cytospins: 10^5 FACS-enriched spleen, blood and GI tract-derived eosinophils (*Il5*-tg) from 7-8 week-old females and males, were resuspended in 100µl 5% FCS-supplemented RPMI media and cytospun for 5 minutes at 50g into a funnel. Slides were air-dry for 30 minutes, fixed with ice-cold methanol for 5 minutes and then left air-dry overnight. Slides were washed, incubated 1h in blocking solution and stained overnight at 4°C with mouse anti-EPX antibody (MM25-82.2.1 1:200, kindly provided by Dr. E.A. Jacobsen from Mayo Clinic, Scottsdale, AZ), followed by 1hour RT incubation with AlexaFluor goat-anti mouse 647. DAPI staining, mounting and imaging were performed as above. EPX staining intensity was quantified across the cell diameter in Fiji (MultiPlot) for 15 cells per condition.

Image analysis for active-to-basal eosinophil ratio quantification

The cores used for quantification as well as patient data are available in Supplementary Table S2. Cores were chosen based on presence of colonic epithelium. ND files were imported in Imaris 9.6.0 and spots objects were created in the green (MBP) and red (PD-L1) channels separately (estimated XY Diameter = 7 µm, estimated Z Diameter = 4 um, Quality Filter > 6). To quantify co-expression of PD-L1 and MBP, the distance of each spot in the green channel to the nearest spot in the red channel was computed. Green spots (eosinophils) with distance to red spots < 4 µm were considered as active eosinophils (co-expressing PD-L1). Green spots with distance to red spots > 4 µm were considered basal eosinophils. The active-to-basal ratio was then computed by dividing the number of active by the number of basal eosinophils in each core. For localization analysis, the active-to-basal ratio in colon crypts of human and mouse tissue was calculated in manually drawn regions of interest comprising the lower (basal) or upper (luminal) thirds.

Histological assessment of colitis

Transversal mid-colon sections (0.5cm) were fixed overnight in buffered 10% formalin solution, followed by paraffin embedding. Sections were stained with haematoxylin/eosin. Histopathology of the colon was scored in a blinded fashion considering four categories (each scored on a scale of 0–3): epithelial hyperplasia/damage and goblet cell depletion; leukocyte infiltration in the *lamina propria*; submucosal inflammation and oedema; area of tissue affected. The final score presented (0-12) represents the sums of all categories.

In vitro genome-wide CRISPR inhibition screen

1.3 billion BMSCs from 10-16 week-old females and males (n = 27, dCas9-KRAB) were isolated as described above. BMSCs were then split in 2 replicates and each lentivirally transduced with an independently amplified genome-wide CRISPR inhibition library[57] (Addgene #83987). 5 days post transduction, BFP^+ BMSCs were FACS-enriched and their culture media supplemented with recombinant IL-5 (10ng/mL, PreproTech). Following 6 days of IL-5-mediated differentiation, BM-Eos were conditioned with colon CM overnight (1:10). $PD\text{-}L1^+CD80^+$ eosinophils were sorted, the genomic DNA extracted and sgRNAs were target amplified. Library size-distribution was measured with the Agilent high sensitivity D5000 assay on a TapeStation 4200 system (5067-5592 Agilent technologies). Sequencing was performed in single-end mode (75 cycles) on Illumina NextSeq. Reads were trimmed with cutadapt[58] and aligned to the sgRNA references with Bowtie2[59]. MAGeCK[60] was used for guide counting and paired testing.

Western blotting

BM-Eos were isolated from 8-10 week-old females and males (B6J), differentiated and flow-cytometry-purified. Cells were conditioned with colon CM (1:10) or rec-IL-33 (20ng/mL PeproTech) for 45 minutes, then lysed in RIPA buffer (R0278 Sigma) supplemented with 2 mM sodium orthovanadate (J60191.AE Thermo Fisher Scientific), 15 mM sodium pyrophosphate (J62052.AK Thermo Fisher Scientific), 10 mM sodium fluoride (447351000 Thermo Fisher Scientific), and 1x complete protease inhibitor cocktail (11836153001 Roche).vProtein concentrations were determined by BCA assay (23227 Pierce), and equal amounts were separated by SDS–PAGE using 10% acrylamide gels followed by transfer onto nitrocellulose membranes (88018 Thermo Fisher Scientific). Membranes were probed with antibodies against vinculin (42H89L44, 700062 Thermo Fisher Scientific), phospho-p38 MAPK (Thr180/Tyr182, MA5-15218 Thermo Fisher Scientific) and phospho-p65 (Ser536, 93H1, 3033 Cell Signalling Technology).

Enzyme-linked immunosorbent assay (ELISA)

Proteins were extracted from colon samples homogenized in 450ul RIPA lysis buffer (Thermo Fisher Scientific) supplemented with Na_3Vo_4 (100mM), NaF (10mM) and Protease inhibitor cocktail (cOmplete, Mini Protease Inhibitor Tablets, 11836153001Roche). The supernatant was collected and centrifugated at maximum speed for 10 minutes at 4°C. Protein concentration was quantified with Pierce BCA Protein Assay Kit (23225, Thermo Fisher Scientific). Plasma was isolated from blood in BD Microtainer tubes (365968, BD). Plates were coated overnight and mouse IL-33 ELISA kit (88-7333-88 Thermo Fisher Scientific) was used to quantify colon and plasma levels of IL-33 according to manufacturer's instructions.

LEGENDplex™ bead-based immunoassay

Proteins were extracted as described above. Colon and plasma levels of IFN-ɣ, IL-22 and TNF-α were quantified using LEGENDplex™ MU Th17 Panel (7-plex) according to manufacturer's instructions.

Molecular Cartography

Sample preparation: fresh frozen UC colon samples (3 patients) were sectioned onto coverslips and processed by Resolve Biosciences.

Segmentation: Cellpose[61] (v. 2.0.4) was used to segment nuclei in the DAPI images with the pretrained nuclei model and flow_threshold 0.5, cellprob_threshold -0.2. The nuclear segments were then expanded by 10 pixel (1.38 µm) using the 'expand_labels' function in scikit-image and transcripts were subsequently assigned to the expanded segments. Segments with less than 3 molecules or 3 genes detected were removed from the analysis.

Segmentation-free approach: To circumvent issues of segmentation we employed a transcript focused approach in which we used spatial clusters of specific marker genes to represent cell types and investigate co-localization. For this, distances between individual transcripts of *CD4, SIGLEC8, CD8A, CD19, FOXP3* and *FCN1* were computed using Euclidean distances of the 2D coordinates. Hierarchical clustering was then applied to the distance matrix with average linkage to prevent chaining and a tree cut at height of 5 µm (hclust in the stats R package). We then utilised a kd-tree based nearest neighbour search to identify the clusters in the surrounding of each other cluster in a pre-defined radius of 10 µm as implemented in the R function 'nn2' (RANN v. 2.6.1, searchtype='radius') with a sufficiently large k (k=41). This approach runs in O(M logM) time and avoids computation of a distance matrix for thousands of objects. Finally, a neighbourhood-graph was constructed from the resulting adjacency matrix where vertices (transcript clusters) are connected by edges if they are no further apart than 10 µm. From this graph the number of edges between different cell types was computed and compared to an empirical null distribution which was derived from randomly permuting the labels of the vertices (m=1000). This approach takes tissue composition and spatial structure into account and allows the computation of P values as $P=(b+1)/(m+1)$ where b is the number of times the permutation produced a more extreme number of edges between two cell types than observed and m the total number of permutations[62]. This was done for each slide and possible cell-cell interaction to derive a score that represents the fraction of images in which a specific interaction was significant, with the sign representing interaction or avoidance; visualisation was adopted from[63].

Graphical illustrations

Schematics of experimental workflows were created using a licenced version of Biorender.com.

Data and Code Availability

Single-cell and bulk RNA-seq data generated during this study are deposited at the Gene Expression Omnibus under access number GSE182001. The code used in this study is available at https://github.com/Moors-Code/Eosinophils_scRNASeq

Methods references

32. Adachi, O. *et al.* Targeted disruption of the MyD88 gene results in loss of IL-1-and IL-18-mediated function. *Immunity* **9**, 143–150 (1998).

33. Hoshino, K. *et al.* Cutting edge: Toll-like receptor 4 (TLR4)-deficient mice are hyporesponsive to lipopolysaccharide: evidence for TLR4 as the Lps gene product. *J. Immunol.* **162**, 3749–3752 (1999).

34. Rawlins, E. L., Clark, C. P., Xue, Y. & Hogan, B. L. M. The Id2+ distal tip lung epithelium contains individual multipotent embryonic progenitor cells. *Development* **136**, 3741–3745 (2009).

35. Dent, L. A., Strath, M., Mellor, A. L. & Sanderson, C. J. Eosinophilia in transgenic mice expressing interleukin 5. *J. Exp. Med.* **172**, 1425–1431 (1990).

36. Lee, H.-M. *et al.* IFNγ signaling endows DCs with the capacity to control type I inflammation during parasitic infection through promoting T-bet+ regulatory T cells. *PLoS Pathog.* **11**, e1004635 (2015).

37. Oboki, K. *et al.* IL-33 is a crucial amplifier of innate rather than acquired immunity. *Proc. Natl. Acad. Sci. U. S. A.* **107**, 18581–18586 (2010).

38. Townsend, M. J., Fallon, P. G., Matthews, D. J., Jolin, H. E. & McKenzie, A. N. T1/ST2-deficient mice demonstrate the importance of T1/ST2 in developing primary T helper cell type 2 responses. *J. Exp. Med.* **191**, 1069–1076 (2000).

39. Lee, J. J. *et al.* Defining a link with asthma in mice congenitally deficient in eosinophils. *Science* **305**, 1773–1776 (2004).

40. Doyle, A. D. *et al.* Homologous recombination into the eosinophil peroxidase locus generates a strain of mice expressing Cre recombinase exclusively in eosinophils. *J. Leukoc. Biol.* **94**, 17–24 (2013).

41. Diehl, G. E. *et al.* Microbiota restricts trafficking of bacteria to mesenteric lymph nodes by CX3CR1hi cells. *Nature* **494**, 116–120 (2013).

42. Wiles, S., Pickard, K. M., Peng, K., MacDonald, T. T. & Frankel, G. In vivo bioluminescence imaging of the murine pathogen Citrobacter rodentium. *Infect. Immun.* **74**, 5391–5396 (2006).
43. Hao, Y. *et al.* Integrated analysis of multimodal single-cell data. *Cell* **184**, 3573–3587.e29 (2021).
44. Korsunsky, I. *et al.* Fast, sensitive and accurate integration of single-cell data with Harmony. *Nat. Methods* **16**, 1289–1296 (2019).
45. Kowalczyk, M. S. *et al.* Single-cell RNA-seq reveals changes in cell cycle and differentiation programs upon aging of hematopoietic stem cells. *Genome Res.* **25**, 1860–1872 (2015).
46. Trapnell, C. *et al.* The dynamics and regulators of cell fate decisions are revealed by pseudotemporal ordering of single cells. *Nat. Biotechnol.* **32**, 381–386 (2014).
47. Cacchiarelli, D. *et al.* Aligning Single-Cell Developmental and Reprogramming Trajectories Identifies Molecular Determinants of Myogenic Reprogramming Outcome. *Cell Syst* **7**, 258–268.e3 (2018).
48. La Manno, G. *et al.* RNA velocity of single cells. *Nature* **560**, 494–498 (2018).
49. Holland, C. H. *et al.* Robustness and applicability of transcription factor and pathway analysis tools on single-cell RNA-seq data. *Genome Biol.* **21**, 36 (2020).
50. Gu, Z., Eils, R. & Schlesner, M. Complex heatmaps reveal patterns and correlations in multidimensional genomic data. *Bioinformatics* **32**, 2847–2849 (2016).
51. Wickham, H. *ggplot2: Elegant Graphics for Data Analysis*. (Springer International Publishing, 2016).
52. Brummelman, J. *et al.* Development, application and computational analysis of high-dimensional fluorescent antibody panels for single-cell flow cytometry. *Nat. Protoc.* **14**, 1946–1969 (2019).

946 53. Dyer, K. D. *et al.* Functionally Competent Eosinophils Differentiated Ex Vivo in High
947 Purity from Normal Mouse Bone Marrow. *The Journal of Immunology* vol. 181 4004–
948 4009 Preprint at https://doi.org/10.4049/jimmunol.181.6.4004 (2008).
949 54. Hatakeyama, M. *et al.* SUSHI: an exquisite recipe for fully documented, reproducible
950 and reusable NGS data analysis. *BMC Bioinformatics* **17**, 228 (2016).
951 55. Robinson, M. D., McCarthy, D. J. & Smyth, G. K. edgeR: a Bioconductor package for
952 differential expression analysis of digital gene expression data. *Bioinformatics* **26**, 139–
953 140 (2010).
954 56. Kolde. pheatmap: Pretty Heatmaps. R package version 1.0. 12. *CRAN. R-project.*
955 *org/package= pheatmap*.
956 57. Horlbeck, M. A. *et al.* Compact and highly active next-generation libraries for CRISPR-
957 mediated gene repression and activation. *Elife* **5**, (2016).
958 58. Martin, M. Cutadapt removes adapter sequences from high-throughput sequencing
959 reads. *EMBnet.journal* **17**, 10–12 (2011).
960 59. Langmead, B. & Salzberg, S. L. Fast gapped-read alignment with Bowtie 2. *Nat.*
961 *Methods* **9**, 357–359 (2012).
962 60. Li, W. *et al.* MAGeCK enables robust identification of essential genes from genome-
963 scale CRISPR/Cas9 knockout screens. *Genome Biol.* **15**, 554 (2014).
964 61. Stringer, C., Wang, T., Michaelos, M. & Pachitariu, M. Cellpose: a generalist algorithm
965 for cellular segmentation. *Nat. Methods* **18**, 100–106 (2021).
966 62. Phipson, B. & Smyth, G. K. Permutation P-values should never be zero: calculating
967 exact P-values when permutations are randomly drawn. *Stat. Appl. Genet. Mol. Biol.* **9**,
968 Article39 (2010).
969 63. Lohoff, T. *et al.* Integration of spatial and single-cell transcriptomic data elucidates
970 mouse organogenesis. *Nat. Biotechnol.* **40**, 74–85 (2022).

End notes

Acknowledgements: We thank S. Baghai Sain, D. Eletto, A. Ozga, F. Mhamedi Baccouche, A. Munitz and A. Müller for technical support and insightful ideas. The authors would also like to thank E.A. Jacobsen and the Mayo Clinic for providing PHIL and Eo-*Cre* mice and the anti-EPX antibody. Sonia Tugues Solsona and Colin Sparano for providing *Id2CreERT2;RosaEYFP* mice. This study was supported by an SNSF Eccellenza Professorial Fellowship from the Swiss National Science Foundation (SNF) to I.C.A. (PCEFP3_187021) and A. E. M (PCEFP3_ 181249); P.K. is supported by grants from the San Salvatore Foundation and the Helmut Horten Foundation. This study was further supported by the Helmsley Charitable Trust grant #1903-03791 to A.E.M. A.G. is supported by fellowship 2450 from the Hartmann-Müller Foundation and 34484 from the Olga Mayenfisch Foundation; I.G.P is supported by fellowship 20C197 from the Novartis Foundation for Medical-Biological Research. T.V. is supported by Czech Science Foundation grant 21-26025S and The project National Institute for Cancer Research (Programme EXCELES, ID Project No. LX22NPO5102) - Funded by the European Union - Next Generation EU; T.V and N.G.N are fellows of the University of Zürich Research Priority Program (URPP) "Translational Cancer Research".

Author contributions: A.G., C.B., I.G.P., N.G.N., D.C., K.H., V.V., A.L., K.S., T.V., D.R., J.G. and V.P. V. performed experiments and analyses. C.B., N.G.N., K.Bach, I.E.A. and K.H. performed bioinformatics analyses. I.C.A., A.E.M., B.B., P.K., C.S., E.S. and K.B. designed and supervised experiments. I.C.A., C.B. and A.G. wrote the manuscript.

Competing interest statement: The authors declare no competing interests.

Additional information: Supplementary information is available for this paper. Correspondence and requests for materials should be addressed to I.C.A or A.E.M. Reprints and permissions information is available at www.nature.com/reprints.

MAIN FIGURE LEGENDS

Fig. 1 | A-Eos and B-Eos are two distinct GI resident eosinophil subsets. a, UMAP of eosinophil transcriptomes obtained from BM, blood, spleen, SI, stomach and colon of *Il5*-tg mice (n = 3). **b,** Eosinophil differentiation trajectory. **c,** Subset distribution across organs (% of eosinophils). **d,** Expression of cluster marker genes. Complete list of cluster markers available in Table S1. **e,** Top: UMAP of *Cd80* and *Cd274* expression. Bottom: expression levels over pseudotime. **f**, Top: UMAP of eosinophil proteomic profiles isolated from blood, spleen, stomach, colon and SI. Bottom: heatmap of median surface marker expression across subsets (n = 5, B6J). **g**, Representative FACS plots of A-Eos (PD-L1$^+$CD80$^+$) and PD-L1$^-$CD80$^-$ eosinophils across organs. Numbers indicate % of eosinophils. **h**, Representative IF of Siglec F and CD80 in the murine colon (n = 3, B6J). Arrows mark Siglec F$^+$ CD80$^+$ A-Eos (red) and Siglec F$^+$ CD80$^-$ B-Eos (green). Nuclei stained with DAPI. Scale bar, 20 µm. **i,** MFI of CD63, SSC-A and Siglec F in colonic A- and B-Eos (n = 6, B6J). Medians are shown. Two-tailed unpaired Student's *t*-test. **j,** Left: Representative images of cytospinned intestinal A- and B-Eos stained with anti-EPX and DAPI (n = 3, *Il5*-tg). Right: quantification of EPX staining intensity at cell periphery and center. Data represents mean ± SD. Two-tailed unpaired Student's *t*-test. **k**, Active-to-basal ratio in luminal third vs. basal third of colonic crypts (n = 3, B6J). Two-tailed paired Student's *t*-test. **l**, Left: Active-to-basal ratio in luminal vs. basal third of colonic crypts of healthy human colon cores (n = 5). Two-tailed paired Student's *t*-test. Right: active-to-basal ratio in healthy (5 patients, 9 cores), CD (5 patients, 9 cores) and UC (4 patients, 8 cores) samples. One-way ANOVA. Data represents mean ± SD. Patient information available in Table S2. In **a, b, e** and **f**, dots represent single cells, colored by cluster identity.

Fig. 2 | *A-Eos have antibacterial and immune regulatory functions.* a-c, A-Eos frequencies in *H. pylori*-infected (stomach, n = 6), *C. rod*-infected (colon, n = 5) and DSS-treated (colon, n = 8) mice relative to uninfected controls (n = 5-10, B6J). a-b, data are pooled from two independent experiments. Medians are shown. Two-tailed unpaired Student's *t*-test. **d,** Percentage of eosinophil subsets across organs at steady state and during infection, as assessed by scRNAseq. **e**, Frequencies of A-Eos after conditioning with colon CM. Input: BM-derived (n = 5, B6J), blood (n = 5, *Il5*-tg) and splenic (n = 5, *Il5*-tg) eosinophils. Data represents mean ± SD. Two-tailed unpaired Student's *t*-test. **f,** A-Eos frequencies among adoptively transferred CD45.2$^+$ eosinophils in colon and spleen of host, 42 hrs post injection (n = 4, CD45.1). Input A-Eos frequency shown as a reference (splenic eosinophils, n = 2, *Il5*-tg). Medians are shown. Two-tailed unpaired Student's *t*-test. **g**, Gene expression over common pseudotime at steady state (gray) and during *C. rod* infection (dark red). Dots indicate single cells, colored by organ (BM, blood and colon). **h**, *C. rod* (ICC180) viability upon exposure to blood, splenic, colonic (n = 3, pooled *Il5*-tg) or conditioned BM-Eos (n = 3, pooled B6J). Technical replicates and medians are shown. Two-tailed unpaired Student's *t*-test. **i**, Expression of MHC-I-restricted antigen processing and presentation signature and IFN-ɣ-regulated genes. Genes used for scores and signatures are listed in Table S3. Data represents mean ± SD. Two-sided Wilcoxon test (n = 3, *Il5*-tg). **j,k**, Proliferation of anti-CD3/CD28-activated, CFSE-labelled naïve CD4$^+$ T cells co-cultured with conditioned splenic (j, Spl) or sorted gastrointestinal (k, GI) A- and B-Eos (n = 7, *Il5*-tg mice). Medians are shown. One-way ANOVA.

Fig. 3 | *A-Eos maturation is induced locally by IL-33.* a, Activity of A-Eos-specific regulons across clusters. **b,** Expression of NF-κB signalling components. **c,** Quantification of pNF-κB p65$^+$ cells in colonic A- and B-Eos (n = 3, B6J). Data represents mean ± SEM. Two-tailed unpaired Student's *t*-test. **d,e,** A-Eos and B-Eos frequencies in antibiotics-treated (n = 16, B6J)

and germ-free (n = 9, B6J) mice relative to controls. d, Data are pooled from two independent experiments. Medians are shown. Two-tailed unpaired Student's *t*-test. **f,** Depleted gene sets in PD-L1^{+}CD80^{+} A-Eos (red) and PD-L1^{-}CD80^{-} eosinophils (grey), relative to BMSCs. Kolmogorov Smirnov test. Dot size indicates gene set size. Dashed line indicates *P = 0.05*. **g,** A-Eos frequencies after conditioning of BM-Eos with IL-33, colon CM and anti-IL-33 (n = 2, pooled B6J). Technical replicates and mean ± SEM are shown. One-way ANOVA. **h,** Colonic A- and B-Eos frequencies in B6J (n = 21) and MyD88$^{-/-}$ (n = 15) mice treated with IL-33, relative to untreated controls. Medians are shown. Two-tailed unpaired Student's *t*-test.

Fig. 4 | *A-Eos co-localize with CD4^{+} T cells in IBD patients.* **a,** Top: Venn diagram of significant DEGs (*FDR < 0.05, logFC > |2|*) in BM-Eos treated with IL-33 and/or IFN-ɣ (n = 4, B6J). All DEGs listed in Table S4. Bottom: expression of subset markers across conditions. Columns are clustered, rows are scaled. **b**, Proliferation of anti-CD3/CD28-activated, CFSE-labelled naïve CD4^{+} T cells co-cultured with BM-Eos conditioned with IL-33 and/or IFN-ɣ (n = 3, B6J). Data are pooled from two independent experiments. Medians are shown. One-way ANOVA. **c**, A-Eos frequencies in mice treated with IL-33 and/or IFN-ɣ (n = 5, B6J). Medians are shown. One-way ANOVA. **d,** A- and B-Eos frequencies in DSS-treated B6J (n = 5) and *Il33*$^{-/-}$ (n = 4) mice. Medians are shown. Two-tailed unpaired Student's *t*-test. **e,** Frequencies of IFN-ɣ, IL-17 and TNF-α expressing colonic CD4^{+} T cells from mice shown in d. Medians are shown. Two-tailed unpaired Student's *t*-test. **f,** Left: Representative H&E-stained colonic sections of mice shown in d. Scale bars, 100 µm. Right: Colitis score assessed by histopathological examination. Medians are shown. Two-tailed unpaired Student's *t*-test. **g,** Representative Molecular Cartography images of human UC samples. Nuclei are stained with DAPI, *CD4*, *SIGLEC8* and *CD80* RNA molecules are rendered in blue, red and yellow, respectively. Scale bar 200 µm. **h,** Pairwise proximity score of transcripts across slides. The score indicates the fraction of slides in which the proximity of a pair of transcripts is significantly higher than expected by chance. *P* values are computed based on a permutation test (see *Methods*). **i,** Mean counts per slide of *CD80* and *NFKB1* transcripts in the proximity (< 10 µm) of *SIGLEC8* transcripts spatially associated with *CD4* molecules vs. *SIGLEC8* molecules not associated with *CD4* molecules. The central line in the boxplot represents the median count per slide, the lower and upper hinge corresponds to the first quartiles and the whisker extends from the hinge to the smallest or largest value no further than 1.5 x IQR from the hinge. Two-sided paired Wilcoxon test (17 ROIs, n = 4 patients).

Extended Data Figure Legends

Extended Data Fig. 1 | scRNAseq reveals five distinct eosinophil subpopulations. a, Experimental workflow of scRNAseq. **b**, UMAP of all sequenced single-cell transcriptomes passing quality control, clustered and annotated manually based on marker gene expression. **c,** Distribution of unique molecular identifiers (nUMI, log10 normalized), genes (nGenes, log10 normalized) and mitochondrial gene fraction (mitoRatio, log10 normalized) per cell across samples. **d,** Expression density of canonical eosinophil marker genes. **e,** Subset organ distribution. Dashed lines indicate eosinophil subsets from Fig 1a. **f,** Significantly enriched (adjusted $P < 0.05$) GSEA terms across clusters. Kolmogorov Smirnov test. **g,** Left: cell cycle score. Middle: stemness score. Right: granulogenesis score. Data represents mean ± SD. Two-sided Wilcoxon test (n = 3, *Il5*-tg). **h,** Expression of cell cycle genes across eosinophil subsets. Rows are genes and columns are single cells, colored by scaled expression. **i,** Expression of *mKi67*, *Epx* and *S100a6* over pseudotime. **j,** Receptor gene expression in A- and B-Eos. **k,** Immune-regulatory score across subsets. Data represents mean ± SD. Two-sided Wilcoxon test (n = 3, *Il5*-tg). Genes used for scores and signatures are listed in Table S3.

Extended Data Fig. 2 | PD-L1 and CD80 expression define active eosinophils in the GI tract. a, GI surface marker gene expression in A- and B-Eos. **b,** UMAP showing the normalised protein expression intensity of eosinophil surface markers (n = 4, B6J). **c,** Frequencies of A-Eos as assessed by flow cytometry (n = 4-6, B6J). Data represents mean ± SEM. One-way ANOVA. Data pooled from two independent experiments. **d,** Mean fluorescence intensity (MFI) of CD9, CD31, CD54 and CD95 across colonic eosinophil subsets. FMO: fluorescence minus one. **e,** Expression of A-Eos markers, normalised to *Gapdh* in A- and B-Eos sorted from the SI (n = 4, *Il5*-tg). Data represents mean ± SEM. Two-tailed unpaired Student's *t*-test. **f,** Frequencies of $CD63^+$, $CD9^+$ and $CD107a^+$ cells in A- and B-Eos as assessed by flow cytometry (n = 6-7, B6J). Data represents mean ± SEM. Two-tailed unpaired Student's *t*-test. Data pooled from two independent experiments. **g,** EPX IF in sorted blood and spleen eosinophils (n = 3, *Il5*-tg). Nuclei are stained with DAPI. Scale bar, 10 µm. **h,** Schematic representation of basal (lower) and luminal (upper) third of the mucosa. **i,** Representative IF images of Siglec F and CD80 in the murine colon (n = 3, B6J). Arrows mark Siglec F^+CD80^+ A-Eos (red) and Siglec F^+CD80^- B-Eos (green). Nuclei are stained with DAPI. Dashed lines delimit the border of luminal and basal third. Scale bar, 20 µm.

Extended Data Fig. 3 | PD-$L1^+CD80^+$ A-Eos are specific to the murine GI and enriched in human IBD. a, Representative FACS plots of PD-$L1^+CD80^+$ and PD-$L1^-$ $CD80^-$ eosinophils (n = 3, B6J). Numbers indicate % of eosinophils. **b, c,** UMAP of eosinophil transcriptomes (shown in Fig. 1a) including those isolated from uterus, lung and adipose tissue (n = 4, *Il5*-tg). Cells colored by organ (b) and by cluster (c). **d,** Subset distribution across organs (% of eosinophils). **e,** List of shared or unique markers ($logFC > 0.5$, P *adjusted* < 0.05) between A-Eos and tissue eosinophils. Non-parameteric Wilcoxon rank sum test (FindMarkers function in Seurat). **f,** Representative FACS plots of PD-$L1^+CD80^+$and PD-$L1^-CD80^-$ eosinophils in HDM- or PBS-treated mice (n = 2, B6J). Numbers indicate % of eosinophils. **g,** Left: Gating strategy used to identify resident (rEos) and inflammatory (iEos) eosinophils as described by[17]. Right: quantification of PD-$L1^+CD80^+$ and PD-$L1^-CD80^-$ eosinophils in rEos and iEos. Medians are shown. **h**, MBP and PD-L1 IF staining of human tissue microarrays. Representative cores from a healthy individual and CD patient are shown (n = 5). Scale bars, 500 µm (core overview) and 10 µm (high magnification insets).

Extended Data Fig. 4 | Challenge infection induces a compositional shift toward the A-Eos cluster. a, Left: Representative FACS plots of the A-Eos and PD-L1$^-$ CD80$^-$ eosinophils. Numbers indicate % of eosinophils. Right: Absolute counts of A-Eos of mice shown in Fig. 2a-c. Medians are shown. Two-tailed unpaired Student's *t*-test. **b**, Data integration of challenge datasets (darkred dots, n = 4, *Il5*-tg). Steady state dataset (gray) used as a reference. Corresponding steady state organs shown in black. **c,** Data integration of DSS dataset (darkgreen dots, n = 3, B6J). Steady state dataset (gray) is used as a reference. Sstate colon shown in black. **d,** UMAP of integrated (left) and merged (right) steady state (gray) and challenge (red dots) datasets. **e**, Left: BM-blood-colon eosinophil Monocle trajectory at steady state and following *C. rod* infection. Each dot represents a single cell colored by cluster identity. Right: RNA velocities (scvelo) in BM, blood and colon dataset as steady state and during *C. rod* infection. **f,** Significant DEGs (*logFC > 0.5, adjusted P < 0.05*) of circulating eosinophils found in the colon vs in the blood of *C. rod*-infected mice. Non-parameteric Wilcoxon rank sum test (FindMarkers function in Seurat). **g**, Single-cell fate probabilities as calculated by CellRank and summarised for each cluster as a pie chart. Arrows represent velocity flow. Cells and pie charts colored by cluster identity. **h**, Top: Workflow of *in vitro* conditioning. Bottom: A-Eos frequencies after conditioning with increasing doses of colon CM. Input: BM-derived (n = 5, B6J), blood (n = 5, *Il5*-tg) and splenic (n = 5, *Il5*-tg) eosinophils. Medians are shown. One-way ANOVA. **i**, Left: EYFP$^+$ eosinophil frequencies over time across organs after single tamoxifen pulse in *Id2CreERT2;RosaEYFP* mice. Data represents mean ± SD. Right: Frequency of A- and B-Eos in colonic EYFP$^+$ eosinophils at day 2 and 4 post tamoxifen injection (n = 3, *Id2CreER^{T2};RosaEYFP*). Medians are shown. Two-tailed unpaired Student's *t*-test. **j**, Antimicrobial and granulogenesis signature expression in A-Eos. **k**, Gene expression over common pseudotime at steady state (gray) and upon *C. rod* infection (dark red). Dots indicate single cells, colored by organ: BM (blue), blood (yellow) and colon (red). **l**, Edu$^+$/Edu$^-$ eosinophil ratio in the colon of *C.rod*-infected and control B6J (n = 5) and *Il5*-tg (n = 3) mice at day 4 post EdU injection. Data represent mean ± SEM. Two-tailed unpaired Student's *t*-test. **m,** Frequencies of eosinophil progenitors (gated as Live CD45$^+$CD11b$^+$IL5Ra$^+$Lin-Sca1$^-$CD34$^+$) in *C.rod*-infected (n = 17) and control (n = 9) B6J mice. Medians are shown. Data pooled from two independent experiments. Two-tailed unpaired Student's *t*-test. **n,** MFI of CD63 in colonic A- and B-Eos of *C.rod*-infected and control mice (n = 6, B6J). Medians are shown. Two-tailed unpaired Student's *t*-test. **o,** EPX IF of sorted-A-Eos of *C.rod*-infected and control mice (n = 5, *Il5*-tg). Nuclei are stained with DAPI. Insets show protrusions. Scale bar, 10 µm.

Extended Data Fig. 5 | A-Eos interact with T cells. a, Ligand-receptor interactions between eosinophils and CD4$^+$ T cells (left) or CD8$^+$ T cells (right) predicted by CellPhoneDB. Dot size and color indicate interaction mean. **b,** Representative H&E-stained colonic sections and **c,** colitis score in B6J (n = 17) and PHIL (n = 13) mice assessed by histopathological examination; data are pooled from two independent experiments. Medians are shown. Two-tailed unpaired Student's *t*-test. Scale bars, 100 µm. **d**, Frequencies of IFN-ɣ, IL-17 and TNF-α-expressing colonic CD4$^+$ T cells of DSS-treated B6J (n = 17) and PHIL (n = 13) mice. Medians are shown. Two-tailed unpaired Student's *t*-test. **e,** Left: CFSE dilution of T cells co-cultured with BM-derived eosinophils conditioned as indicated and loaded with ovalbumin (OVA) peptide. Right: Representative FACS plots of the CFSE dilution. Numbers indicate % of CFSE dilution (n = 3, B6J). Data represents mean ± SEM. Two-tailed unpaired Student's *t*-test. **f,** Left: A-Eos (PD-L1$^+$CD80$^+$) and B-Eos (PD-L1$^-$CD80$^-$) frequencies in stomach, colon and SI of B6J (n = 5) and *Il5*-tg (n = 5) mice. Medians are shown. Two-tailed unpaired Student's *t*-test. Right:

Representative FACS plots. Numbers indicate % of eosinophils. **g,** UMAP of B6J colonic eosinophils (orange) at steadystate (n = 6) and during *C.rod* infection (n = 5) integrated in the *Il5*-tg dataset (gray). *Il5*-tg colonic eosinophils at steadystate and during *C.rod* infection in black. **h,** Antimicrobial signature, IFN-ɣ-regulated gene signature and antigen processing and presentation via MHC-I in B6J colon and B6J colon + *C.rod*. Data represents mean ± SD. Two-sided Wilcoxon test (n = 3). **i,** A-Eos frequencies in *H. pylori*-infected (stomach, n = 5) and *C. rod*-infected (colon, n = 4-7) B6J and *Il5*-tg mice, relative to uninfected controls. Medians are shown. Two-tailed unpaired Student's *t*-test. **j,k** Absolute counts of A-Eos and B-Eos in colon and SI of B6J mice treated with anti-IL-5 (j, n = 5) or anti-CCR3 (k, n = 5) neutralising antibodies and the respective isotype control. Medians are shown. Two-tailed unpaired Student's *t*-test.

Extended Data Fig. 6 | A-Eos are induced by NF-κB signalling. a, Regulon activity across clusters. **b**, Representative regulons projected on UMAP plot. Cells are colored by binary regulon activity. **c**, Pathway activity across clusters according to PROGENy analysis. **d**, Gene expression relative to *Hprt* measured by qRT-PCR of eosinophils sorted from the blood (n = 6), spleen (n = 6) and colon (n = 4) of *Il5*-tg mice. Data represents mean ± SEM. One-way ANOVA. **e,** Representative images of pNF-κB p65 IF staining in colonic eosinophils (n = 3, B6J). Arrows mark A-Eos (Siglec F^+ $CD80^+$, red) and B-Eos (Siglec F^+ $CD80^-$, green). Nuclei are stained with DAPI. Scale bar, 20 µm. **f**, A-Eos frequencies upon conditioning of BM-Eos with colon CM and/or NF-κB inhibitor (n = 5, B6J). Data represents mean ± SD. One-way ANOVA. **g,** Representative FACS plots of colonic A-Eos (PD-$L1^+CD80^+$) and PD-$L1^-CD80^-$ (B-Eos), relative to Fig 3d. Numbers indicate % of eosinophils. **h,** Left: Representative FACS plots of colonic A-Eos (PD-$L1^+CD80^+$) and PD-$L1^-CD80^-$ (B-Eos), relative to Fig 3e. Numbers indicate % of eosinophils. Right: MFI of Siglec F and % CD63 in colonic A- and B-Eos shown in Fig. 3e. Medians are shown. Two-tailed unpaired Student's *t*-test. **i**, Colonic A- and B-eos frequencies at steady state in B6J (n = 5) $Tlr2^{-/-}$ (n = 3) and $Tlr4^{-/-}$ (n = 7) mice. Medians are shown. One-way ANOVA.

Extended Data Fig. 7 | IL-33 induces the accumulation of A-Eos in the colon. a, Experimental workflow of the CRISPR inhibition screen. **b**, Log10 negative score per gene, as calculated by MAGeCK. *Cd80* and *Cd274* evidenced in orange. Genes involved in TNF-α signalling pathway via NF-κB in red, and MAPK signalling pathway in darkred. **c,** IL-33 concentrations measured by ELISA in colon of DSS-treated mice (n = 12, B6J) and colon and blood of *C.rod* infected mice (n = 7, B6J), compared to untreated controls (n = 7, B6J). Medians are shown. Two-tailed unpaired Student's *t*-test. **d,** IFN-ɣ, TNF-α and IL-22 concentrations measured by LEGENDplex in colon (left) and blood (right) of *C.rod* infected mice (n = 7, B6J), compared to untreated controls (n = 7, B6J). Medians are shown. Two-tailed unpaired Student's *t*-test. **e**, A-Eos (PD-$L1^+CD80^+$) frequencies upon conditioning of BM-Eos with colon CM, IL-22, IL-25, TNF-α or IL-33 (n = 4, B6J). Data are pooled from two independent experiments. Medians are shown. One-way ANOVA. **f**, A-Eos frequencies after conditioning with increasing doses of IL-33. Input: BM-derived (n = 5, B6J), blood (n = 5, *Il5*-tg) and splenic (n = 5, *Il5*-tg) eosinophils. Medians are shown. One-way ANOVA. **g**, Western blot of phospho-p38 and phospho-p65 upon conditioning of BM-Eos with colon CM or IL-33 (n = 3, B6J). **h**, Gene expression normalised to *Hprt* measured by qRT-PCR of BM-Eos upon conditioning with IL-33 (n = 4, B6J). Data represents mean ± SEM. Two-tailed unpaired Student's *t*-test. **i**, ST2 expression in BM-Eos upon IL-33 treatment (n = 4, B6J). Data represents mean ± SEM. Two-tailed unpaired Student's *t*-test. **j**, ST2 expression in colonic A- and B-Eos (n = 5, B6J). Data represents mean ± SEM. Two-tailed unpaired Student's *t*-test. **k**, ST2 expression across organs (n = 5, B6J). Data represents mean ± SEM. One-way ANOVA. **l**, A-Eos frequencies

upon conditioning of WT (n = 2, pooled B6J) or ST2$^{-/-}$ (n = 2, pooled) BM-Eos with colon CM or IL-33. Technical replicates and mean ± SEM are shown. Two-tailed unpaired Student's *t*-test. **m**, Left: Representative FACS plots of A-Eos (PD-L1^{+} CD80^{+}) and PD-L1^{-}CD80^{-} eosinophils in the blood (top) and spleen (bottom). Numbers indicate % of eosinophils. Right: A-Eos frequencies in mice treated with IL-33 (n = 6-7, B6J). Medians are shown. Two-tailed unpaired Student's *t*-test. **n**, A-Eos and B-Eos frequencies in the indicated organs of B6J (n = 7) and *Il33*$^{-/-}$ (n = 5) mice at steady state. Medians are shown. Two-tailed unpaired Student's *t*-test.

Extended Data Fig. 8 | *A-Eos co-localize with CD4^{+} T cells in human IBD.* **a,** Regulon activity in A-Eos across conditions (n = 4, *Il5*-tg). **b,** MDS plot of bulk RNASeq samples shown in Fig.4a. **c,** Heatmap of signature gene expression across conditions of samples shown in Fig. 4a. **d,** A-Eos (PD-L1^{+}CD80^{+}) frequencies upon treatment of BM-Eos with IL-33 and/or IFN-ɣ. (n = 4, B6J). Data represents mean ± SEM. One-way ANOVA. **e,** EPX IF of A-Eos upon exposure to IFN-ɣ for 90 minutes. Splenic eosinophils were magnetically enriched (n = 2, *Il5*-tg), treated overnight with colon CM and A-Eos sorted by flow cytometry. Scale bar, 10 µm. **f,** Frequencies of PD-L1^{+} and CD80^{+} in colonic eosinophils of WT (n = 6, B6J) and Eo-*Cre;Ifngr*$^{fl/fl}$ mice (n = 4) upon *C.rod* infection, relative to uninfected controls (n = 2, B6J). Medians are shown. Two-tailed unpaired Student's *t*-test. **g,** Left: UMAP of single-cell eosinophil transcriptomes isolated from the colon of anti-IFN-ɣR-treated, *C.rod*-infected or control *Il5*-tg mice (n = 3). Middle: expression of IFN-ɣ target genes. Right: Expression of granule and antimicrobial signatures. Data represents mean ± SD. Two-sided Wilcoxon test. **h**, Observed vs. expected number of contacts between clusters of *SIGLEC8* and *CD4* molecules shown per slide. P Values are computed based on a two-sided permutation test (see *Methods*). **i,** Proportions of segmented cells expressing *SIGLEC8* only (blue) or co-expressing both *SIGLEC8* and *CD4* (red) across slides. Dotted horizontal line shows mean. **j,** Mean count per slide of molecules of a given transcript in the proximity (<10 µm) of *SIGLEC8* RNA molecules spatially associated with *CD4* molecules vs *SIGLEC8* molecules not associated with *CD4* molecules. The central line in the boxplot represents the median count per slide, the lower and upper hinge corresponds to the first quartiles and the whisker extends from the hinge to the smallest or largest value no further than 1.5 x IQR from the hinge. Two-sided paired Wilcoxon test (17 ROIs, n = 4 patients).

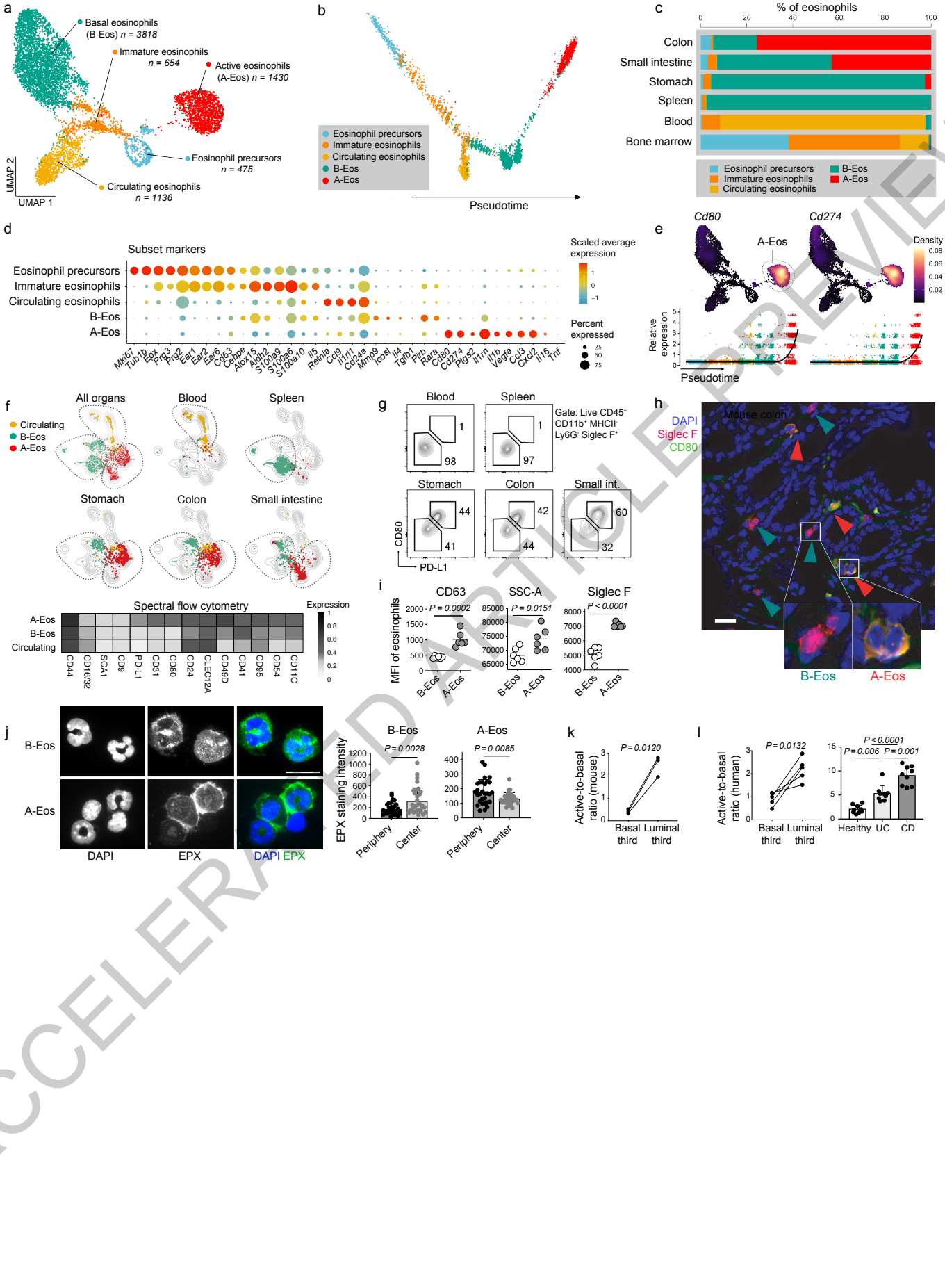

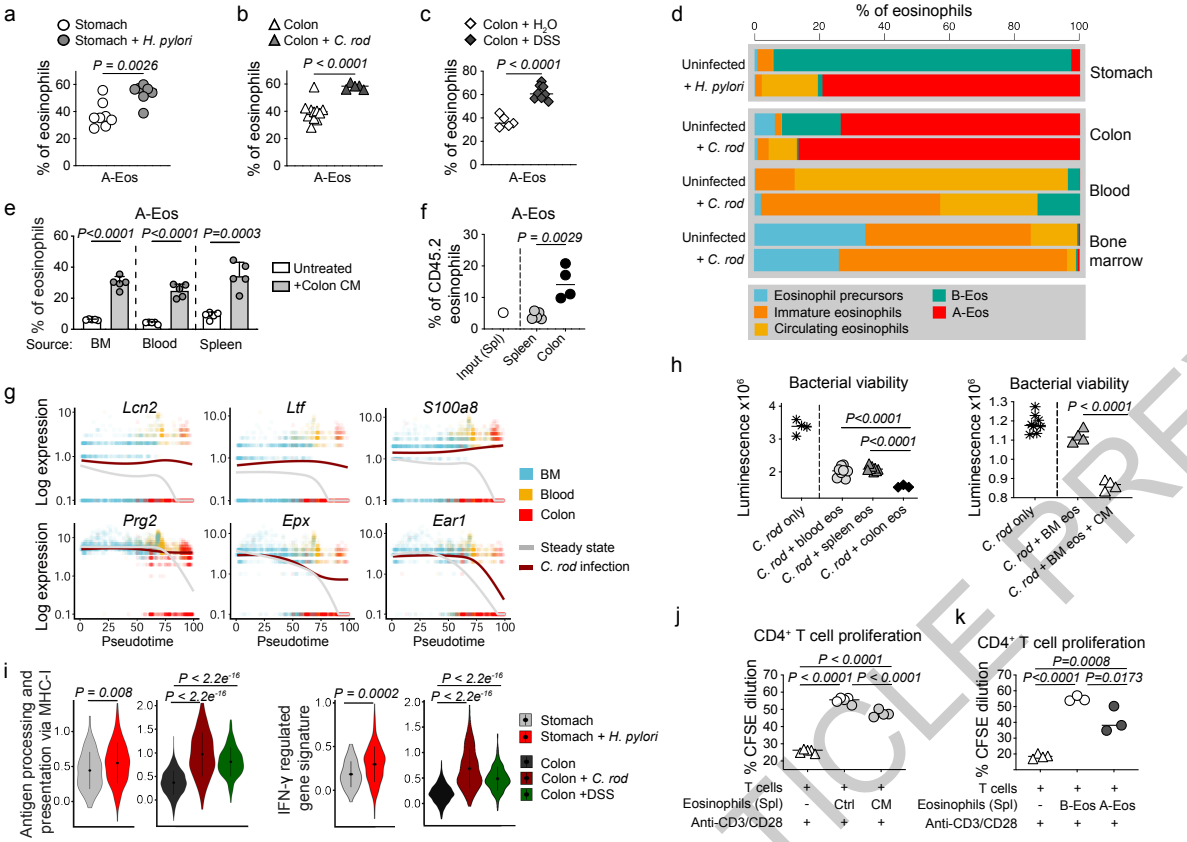

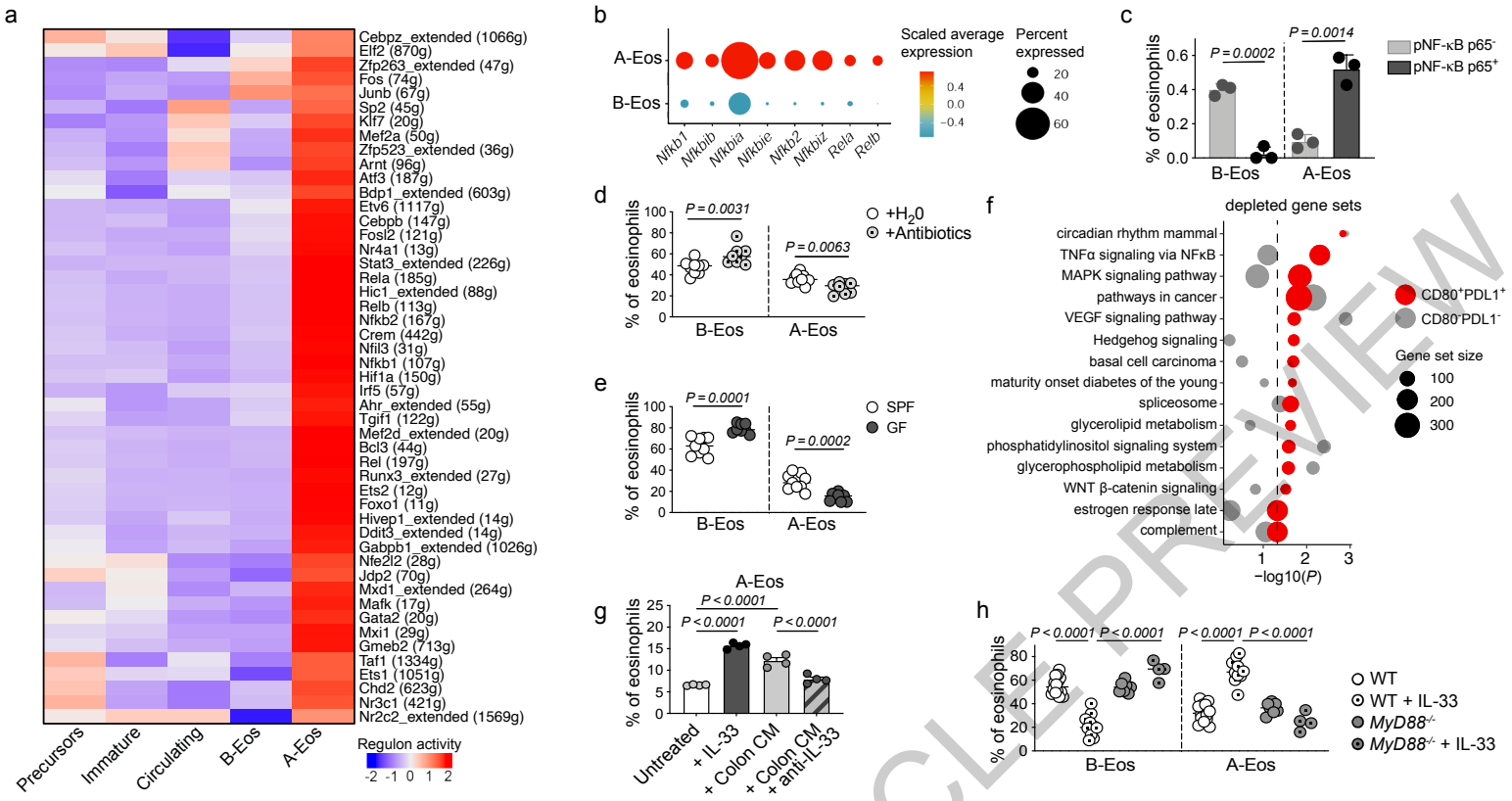

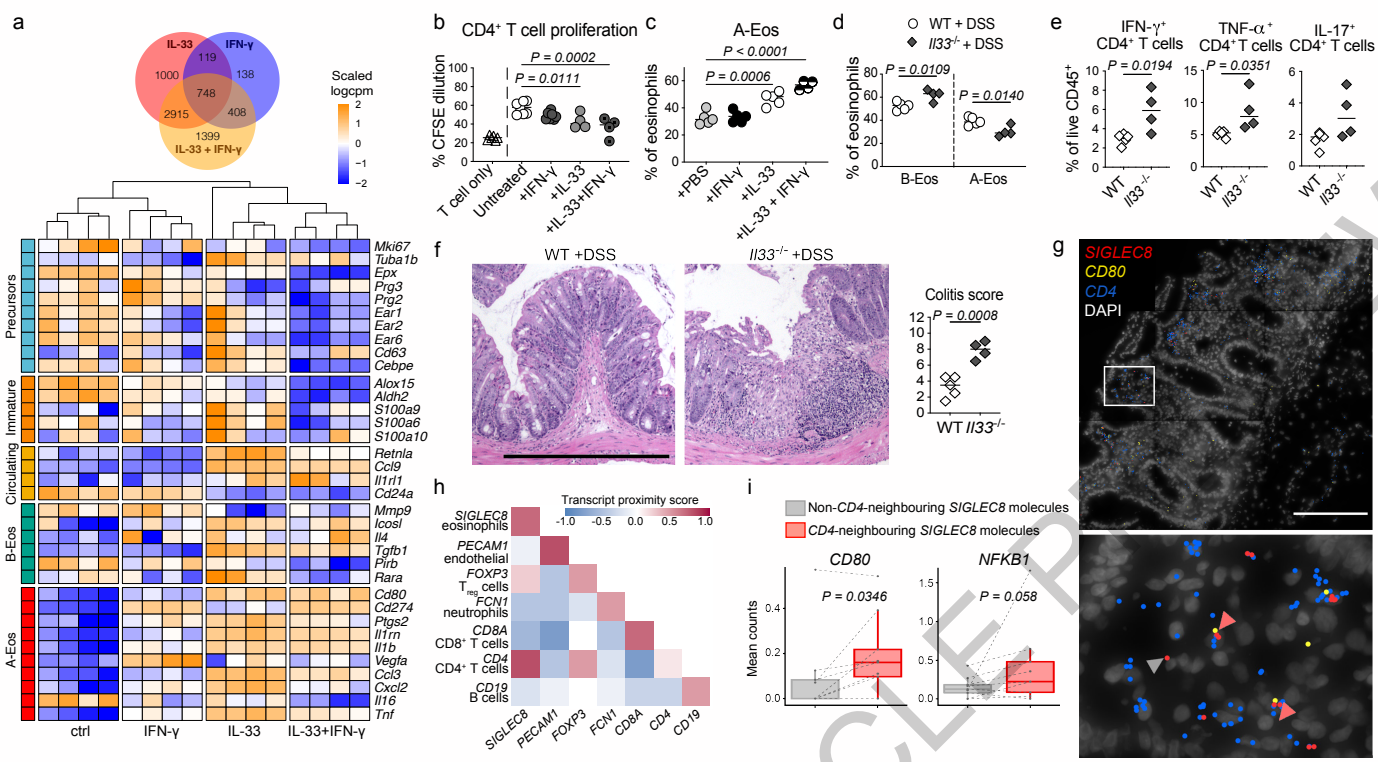

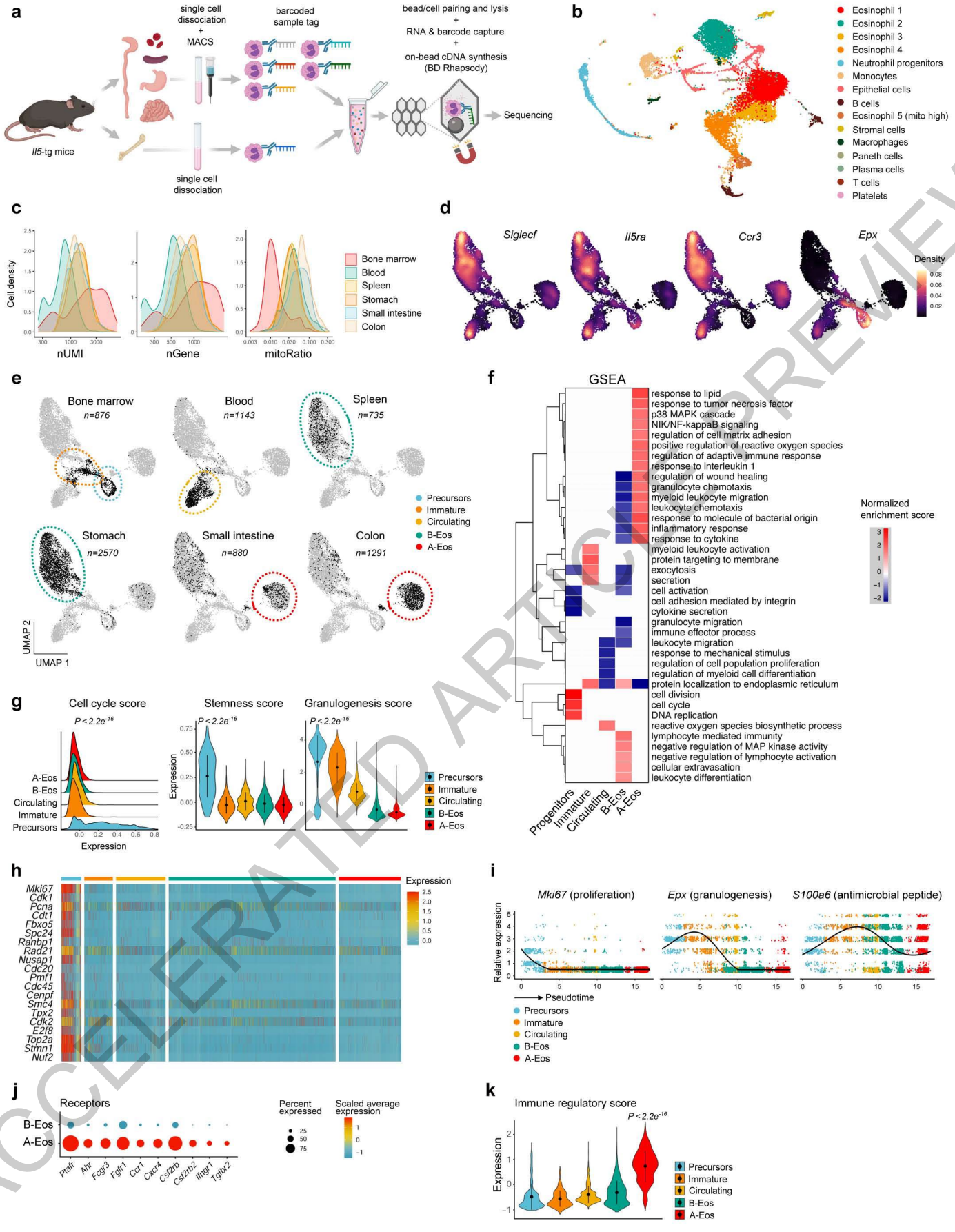

Extended Data Fig. 1

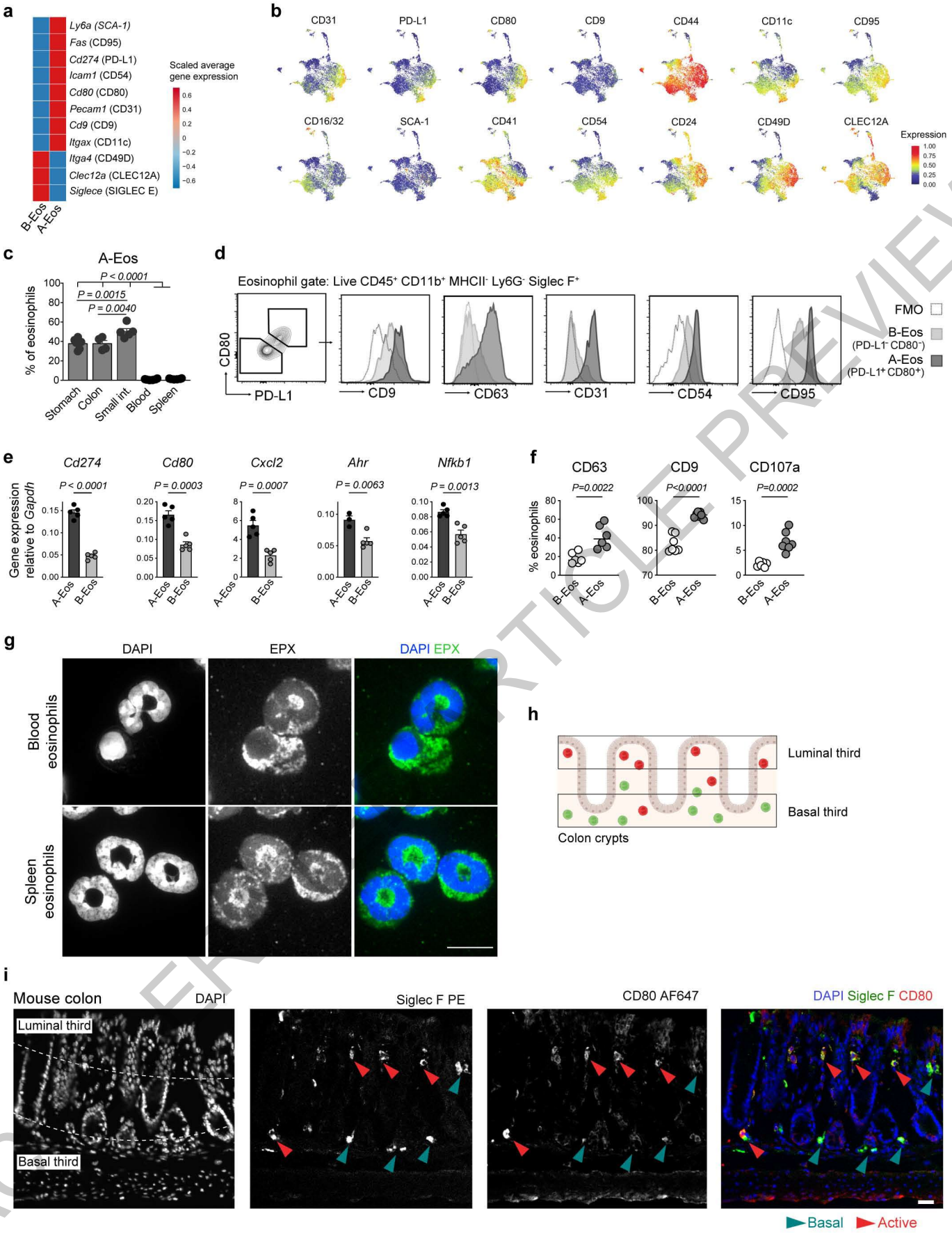

Extended Data Fig. 2

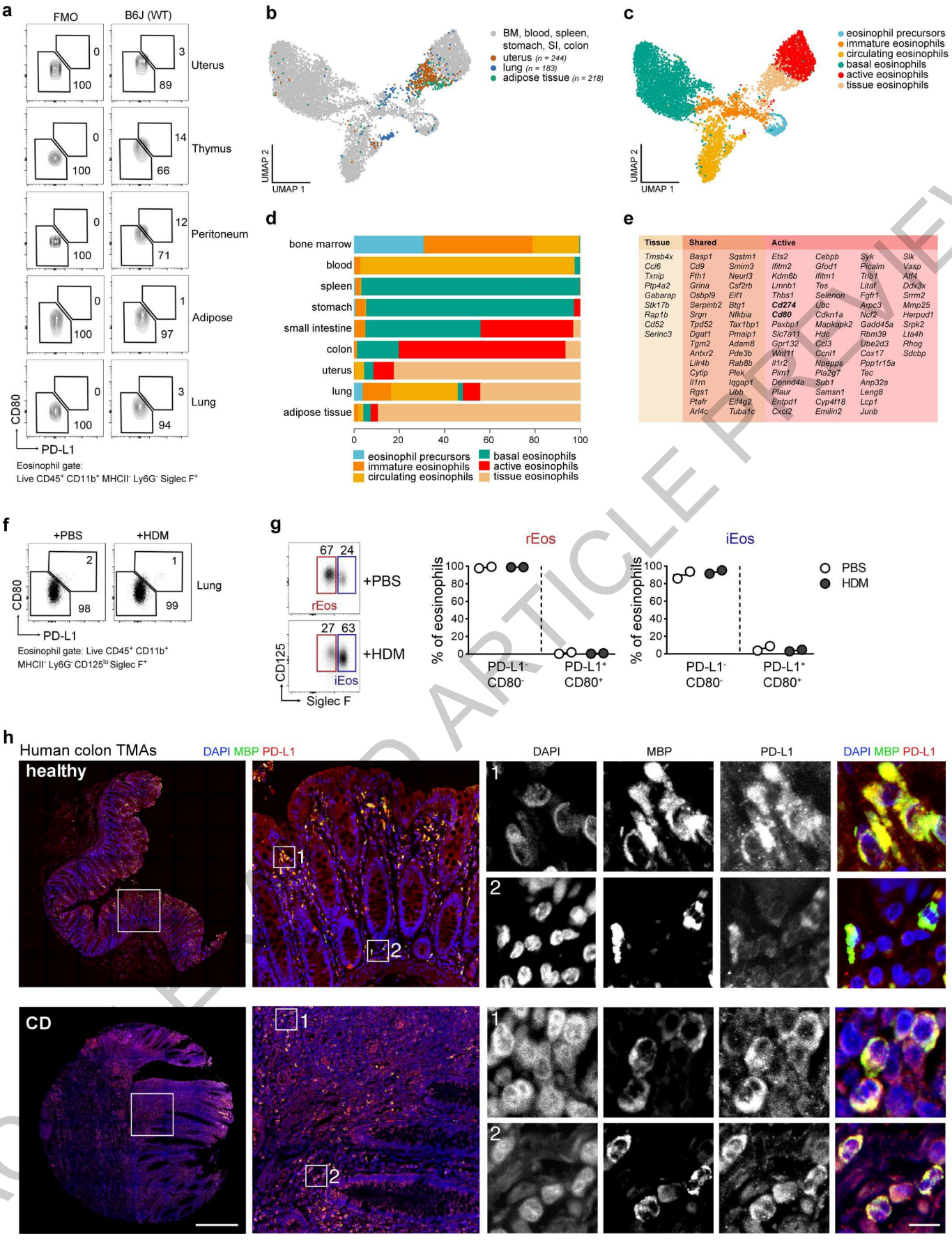

Extended Data Fig. 3

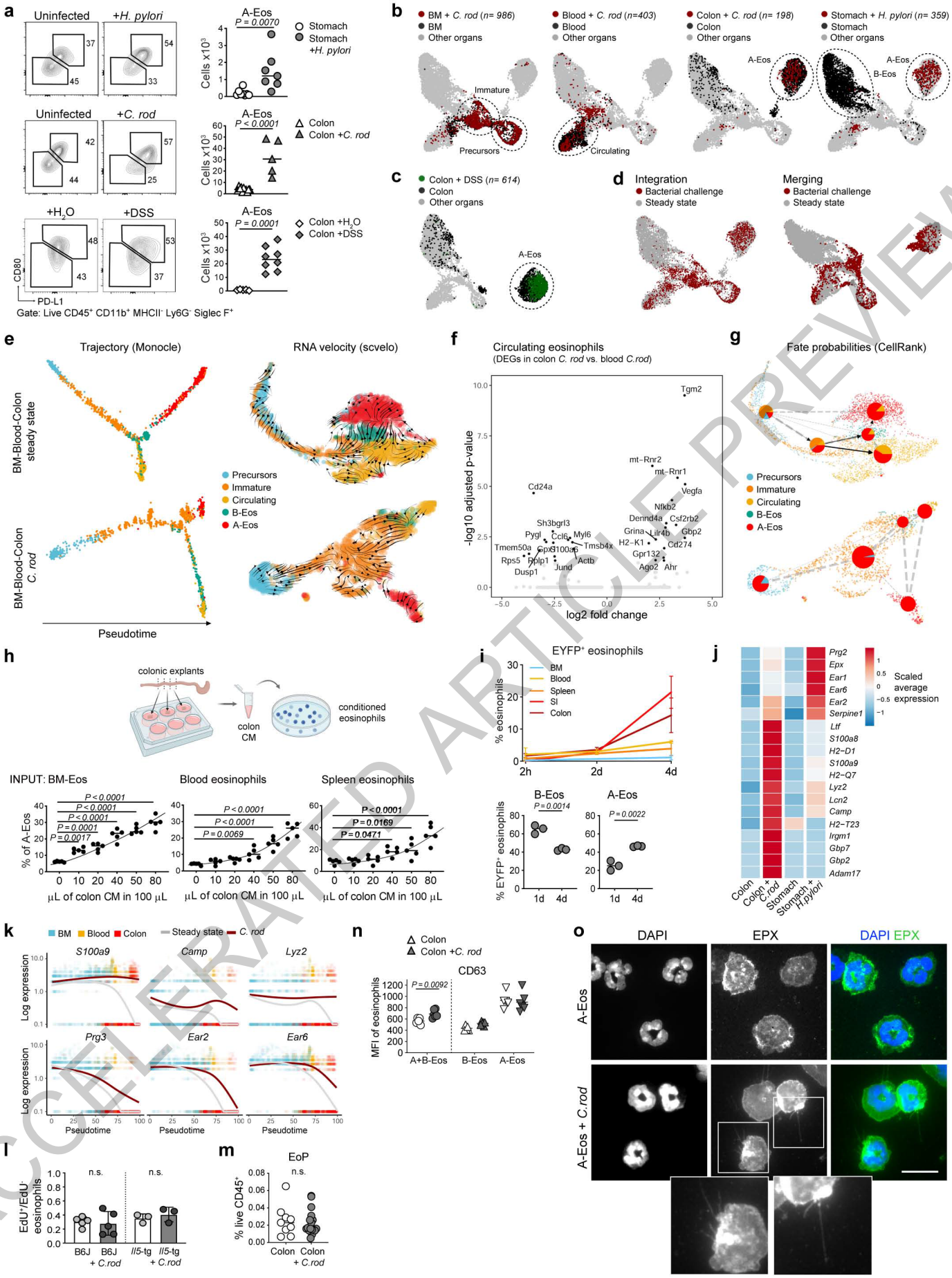

Extended Data Fig. 4

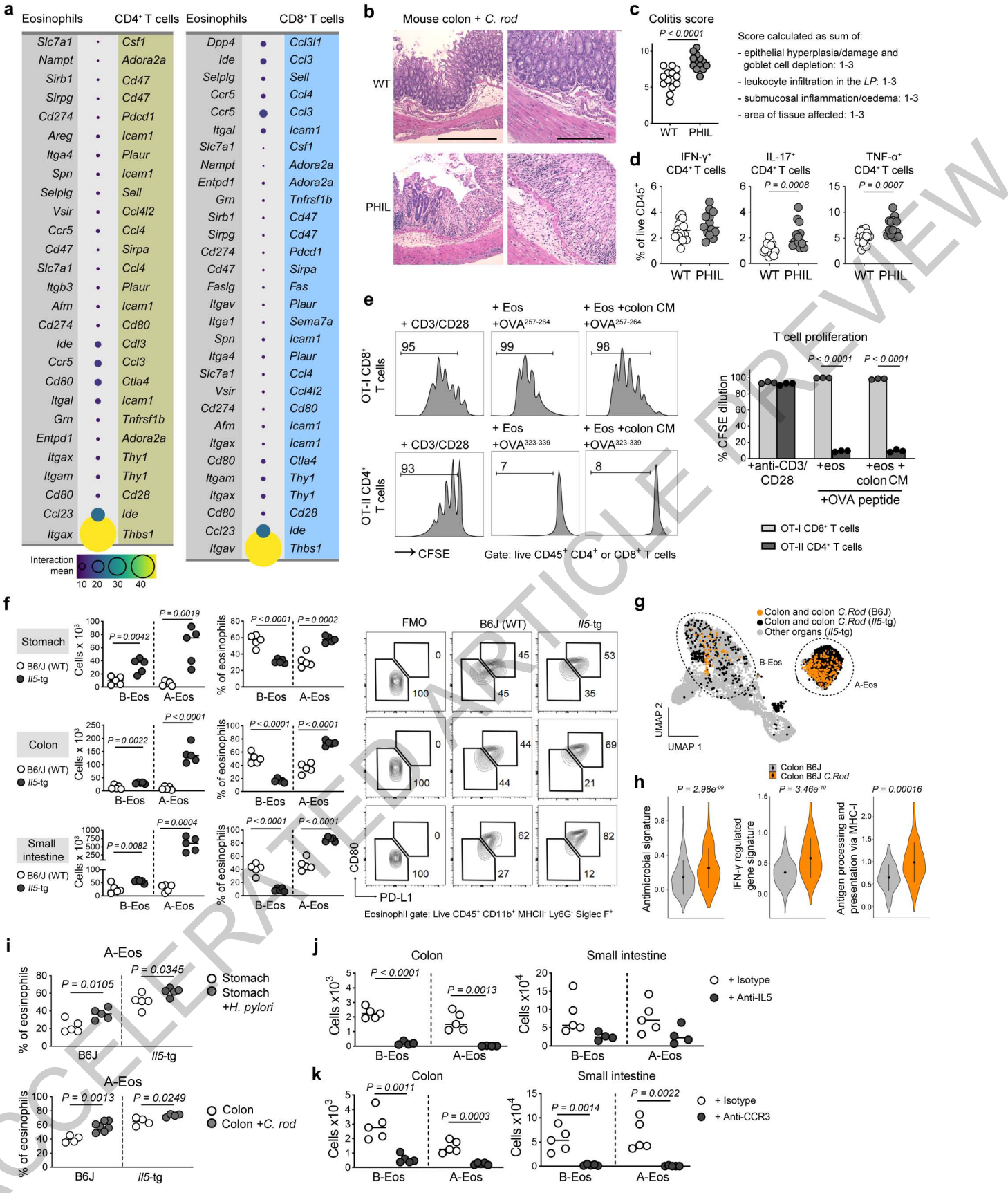

Extended Data Fig. 5

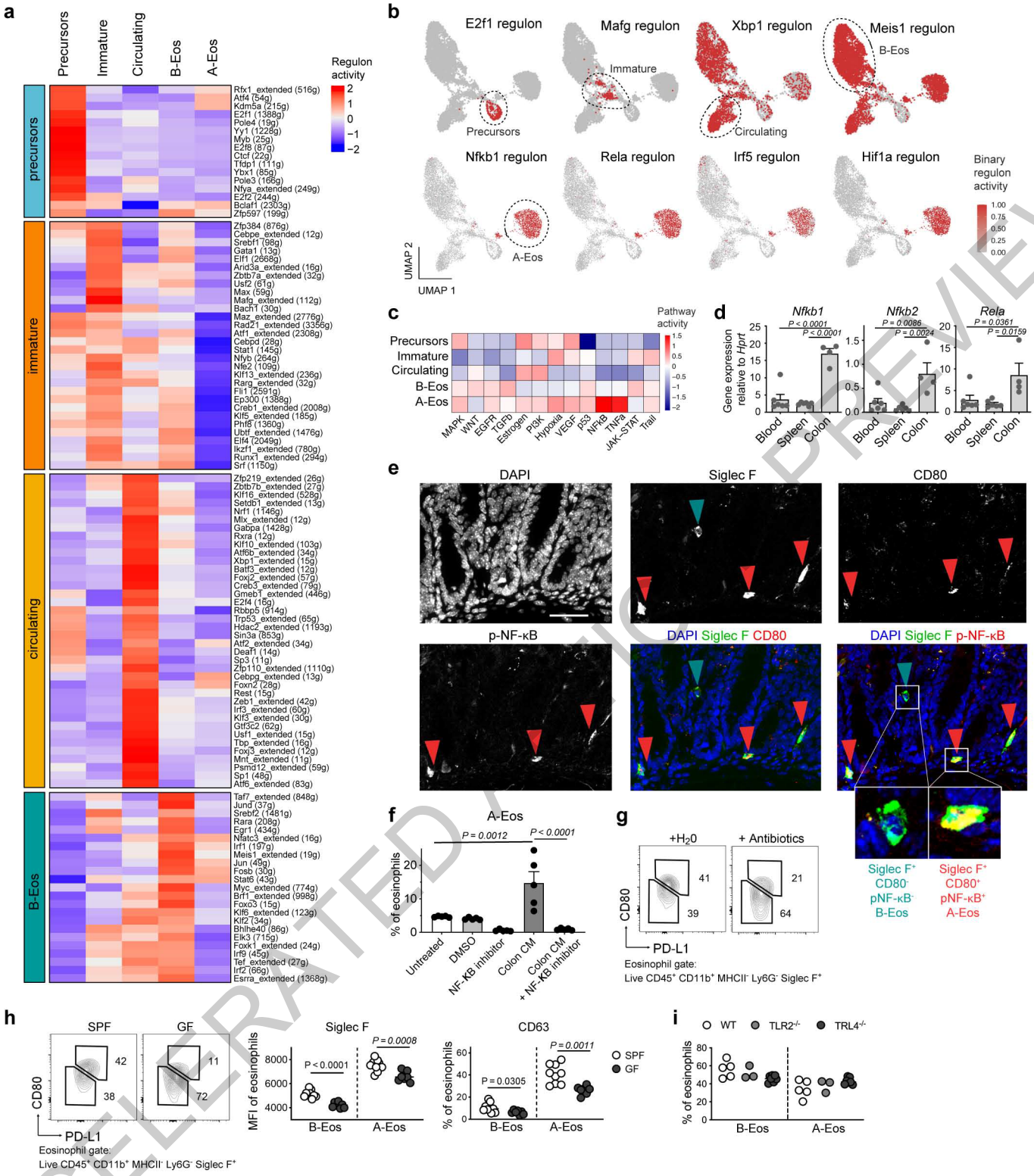

Extended Data Fig. 6

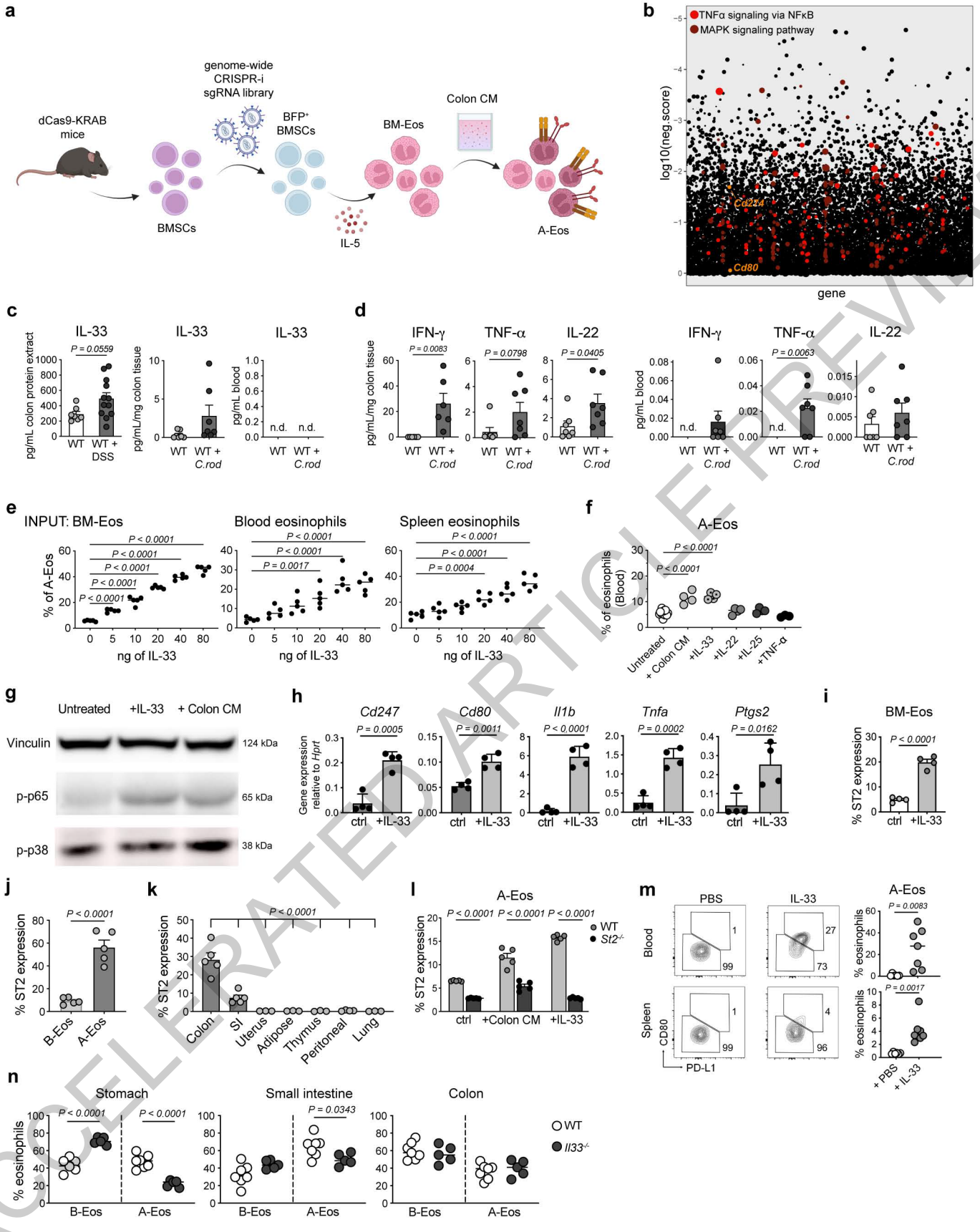

Extended Data Fig. 7

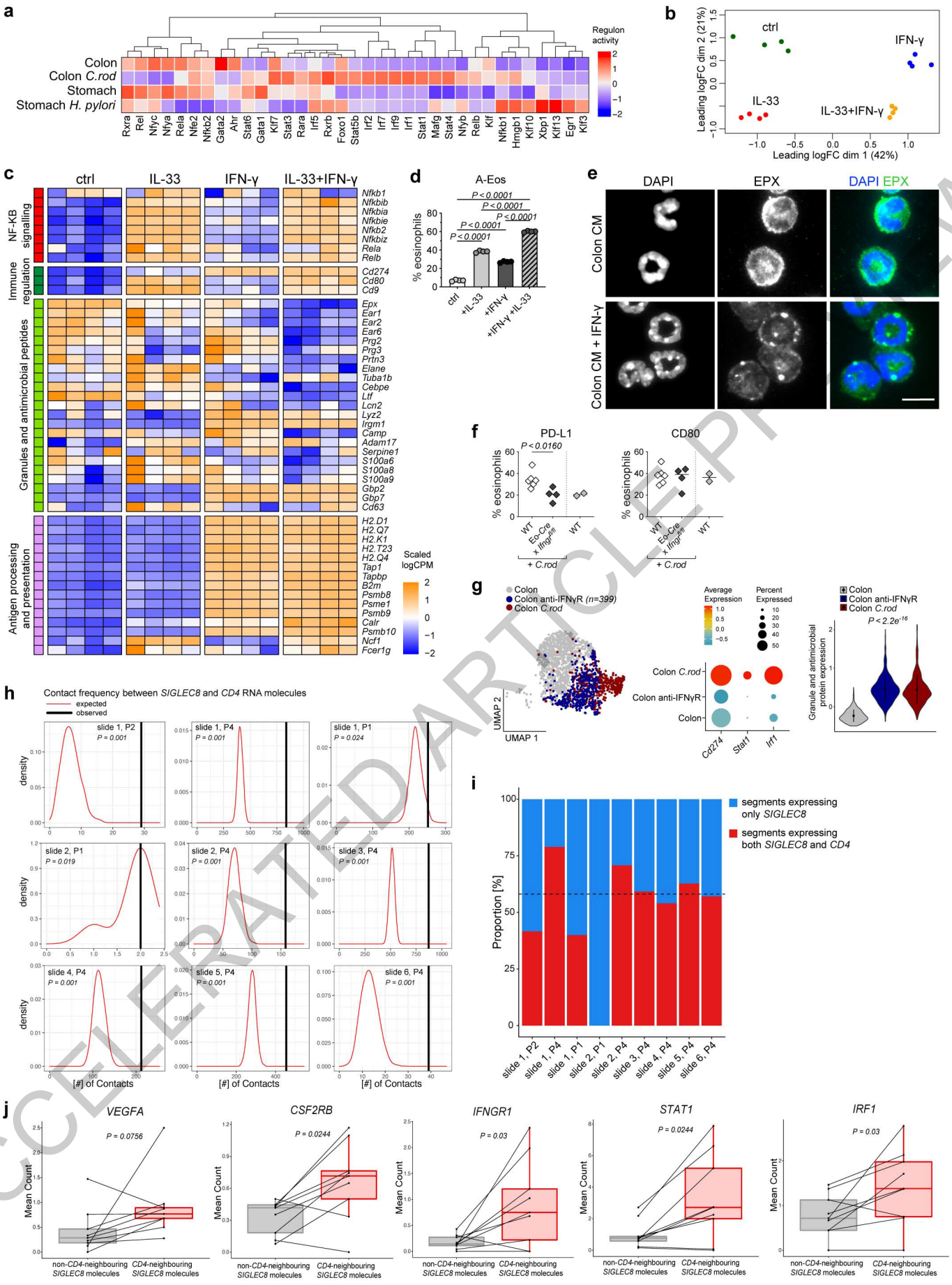

Extended Data Fig. 8

nature portfolio

Corresponding author(s): Isabelle C. Arnold, Andreas E. Moor

Last updated by author(s): Nov 14, 2022

Reporting Summary

Nature Portfolio wishes to improve the reproducibility of the work that we publish. This form provides structure for consistency and transparency in reporting. For further information on Nature Portfolio policies, see our Editorial Policies and the Editorial Policy Checklist.

Statistics

For all statistical analyses, confirm that the following items are present in the figure legend, table legend, main text, or Methods section.

n/a	Confirmed
☐	☒ The exact sample size (*n*) for each experimental group/condition, given as a discrete number and unit of measurement
☐	☒ A statement on whether measurements were taken from distinct samples or whether the same sample was measured repeatedly
☐	☒ The statistical test(s) used AND whether they are one- or two-sided *Only common tests should be described solely by name; describe more complex techniques in the Methods section.*
☒	☐ A description of all covariates tested
☐	☒ A description of any assumptions or corrections, such as tests of normality and adjustment for multiple comparisons
☐	☒ A full description of the statistical parameters including central tendency (e.g. means) or other basic estimates (e.g. regression coefficient) AND variation (e.g. standard deviation) or associated estimates of uncertainty (e.g. confidence intervals)
☐	☒ For null hypothesis testing, the test statistic (e.g. *F*, *t*, *r*) with confidence intervals, effect sizes, degrees of freedom and *P* value noted *Give P values as exact values whenever suitable.*
☒	☐ For Bayesian analysis, information on the choice of priors and Markov chain Monte Carlo settings
☒	☐ For hierarchical and complex designs, identification of the appropriate level for tests and full reporting of outcomes
☒	☐ Estimates of effect sizes (e.g. Cohen's *d*, Pearson's *r*), indicating how they were calculated

Our web collection on statistics for biologists contains articles on many of the points above.

Software and code

Policy information about availability of computer code

Data collection	No software was used.
Data analysis	GraphPad Prism v9.1.1 GraphPad Software Schneider https://www.graphpad.com/scientific- software/prism/ R software v3.6.3 or v4.1.0 GNU project https://www.r-project.org R Studio Server v1.4.1717 https://www.rstudio.com Bcl2fastq v2.20.0.422 (Illumina https://support.illumina.com/sequencing/sequencing_software/bcl2fastq-conversion-software.html) Seven Bridges Genomics (BD Biosciences, https://www.sevenbridges.com) edgeR v3.36.0 R package Robinson et al, 2010 https://bioconductor.org/packages/release/bioc/html/edgeR.html pheatmap v1.0.12 R package Kolde, 2012 https://cran.r-project.org/web/packages/pheatmap/pheatmap.pdf Seurat v4.03 Hao et al, 2021 https://satijalab.org/seurat/get_ started.html RRID:SCR_016341 msigdbr v7.5.1 R package R Bioconductor https://cran.r-project.org/web/packages/msigdbr/vignettes/msigdbr-intro.html fgsea v1.20.0 R package Sergushichev et al, 2016 https://bioconductor.org/packages/release/bioc/html/fgsea.html ggplot2 v3.3.6 R package Wickham, 2016 https://cloud.r-project.org/web/packages/ggplot2/index.html monocle v2.3.6 R package, Trapnell et al, 2014 CellPhoneDB v2.0.0 R package, Efremova et al, 2020 ComplexHeatmap v2.10.0 R package Gu et al, 2016 SCENIC v1.2.4 R package, Aibar et al, 2017 PROGENy v1.13.2 R package, Holland et al, 2020 Biomart v2.50.3 R package v2.46.3 kplots v1.1.14 R package FlowSOM v3.16 R package, Brummelman et al, 2019 Image J v2.0.0 Fiji Schindelin et al, 2012 https://imagej.net/Fiji/ FlowJo v10.7.1 (Becton Dickinson & Company)

BD FACSDiva Software v8.0.2 (BD Biosciences)
cutadapt v4.1, Martin et al 2011
Bowtie2 v2.5.0, Langmead et al, 2012
MAGeCK v0.5.9, Li et al, 2014
velocyto v0.17.16, La Manno et al, 2018
scvelo v0.2.0, Bergen et a, 2020
Cellrank v1.5.1, Lange et al, 2022
SUSHI framework, FGCZ, Hatekeyama et al, 2016
Cellpose, v2.0.4, Stringer et al, 2021
stats, v4.3.0, R package R Core Team, 2013
Code is available at https://github.com/Moors-Code/Eosinophils_scRNASeq

For manuscripts utilizing custom algorithms or software that are central to the research but not yet described in published literature, software must be made available to editors and reviewers. We strongly encourage code deposition in a community repository (e.g. GitHub). See the Nature Portfolio guidelines for submitting code & software for further information.

Data

Policy information about availability of data

All manuscripts must include a data availability statement. This statement should provide the following information, where applicable:

- Accession codes, unique identifiers, or web links for publicly available datasets
- A description of any restrictions on data availability
- For clinical datasets or third party data, please ensure that the statement adheres to our policy

ScRNA-seq data generated during this study are deposited at the Gene Expression Omnibus under access number GSE182001. Gene Ontology databases were downloaded through the R package msigdbr.

Field-specific reporting

Please select the one below that is the best fit for your research. If you are not sure, read the appropriate sections before making your selection.

☒ Life sciences ☐ Behavioural & social sciences ☐ Ecological, evolutionary & environmental sciences

For a reference copy of the document with all sections, see nature.com/documents/nr-reporting-summary-flat.pdf

Life sciences study design

All studies must disclose on these points even when the disclosure is negative.

Sample size	In accordance with the 3Rs, the smallest sample size was chosen that could give a significant difference. Given the robustness of the phenotypes across all methods used (transcriptome and protein level), the minimum sample size assuming no overlap in control versus experimental is three animals per experiment.
Data exclusions	No animals were excluded, unless data acquisition quality was insufficient.
Replication	Mouse experimental data was combined from independent experiments (at least 3 mice) with treated on different days and analyzed together. Micrographs of murine and human colon as well as cytospins are representative of at least two independent experiments. The results were consistent in all independent experiments.
Randomization	All experiments were performed on 6-16 week-old male and female mice, without separation between experimental groups and littermate controls. All samples were analyzed equally without sub-sampling, hence no randomization was required.
Blinding	The researcher was blinded to the genotype during the processing and analysis.

Reporting for specific materials, systems and methods

We require information from authors about some types of materials, experimental systems and methods used in many studies. Here, indicate whether each material, system or method listed is relevant to your study. If you are not sure if a list item applies to your research, read the appropriate section before selecting a response.

Materials & experimental systems

n/a	Involved in the study
☐	☒ Antibodies
☒	☐ Eukaryotic cell lines
☒	☐ Palaeontology and archaeology
☐	☒ Animals and other organisms
☒	☐ Human research participants
☒	☐ Clinical data
☒	☐ Dual use research of concern

Methods

n/a	Involved in the study
☒	☐ ChIP-seq
☐	☒ Flow cytometry
☒	☐ MRI-based neuroimaging

Antibodies

Antibodies used

For surface staining, cell were stained with fixable viability dye eFluor 780 (1:1000, 65-0865-14 eBioscience) and a combination of the following antibodies (1:200, all from BioLegend unless stated otherwise): anti-mouse CD45 BV650 (30-F11, 103151), CD11b BV510 (M1/70, 101263), MHC-II AF700 (M5/114.15.2, 107622), Ly6G Percp-Cy5.5 (1A8, 127616), CD4 PerCP (RM4-5, 100538), TCRβ PE-Cy7 (H57-597, 109222), TCRβ PE-Cy7 (H57-597, 109228), CD80 BV605 (1:100, 16-10A1, 104729), PD-L1 PE-Cy7 (1:100, 10F.9G2, 124314), CD31 PE (390, 102408), CD45.2 BV785 (1:50, 104, 109839), CD9 PE (MZ3, 124805), CD54 BV711 (YN1/1.7.4, 116143), CD63 PE (1:100, NVG-2, 143904), CD95 PE-Cy7(SA367H8, 152607), SiglecE PE (M1304A01, 677104), Sca-1 AF488 (D7, 108116), Sca-1 AF700 (D7, 108142), C-kit BV605 (ACK2, 135121), CD11c APC-Cy7 (N418, 117323), Clec12a PE (5D3, 143404), CD49d FITC (R1-2, 103605), CD16/32 FITC (S17012B, 101305), CD3e Percp-Cy5.5 (145-2C11, 100328), CD8a APC (53-6.7, 100712), NK1.1 Percp-Cy5.5 (PK136, 108727), B220 Percp-Cy5.5 (RA3-6B2, 103236), Ter119 Percp (TER-119, 116227), Gr1 Percp (RB6-8C5, 108427), CD34 AF647 (RAM34, 560230), Siglec F BV421 (E50-2440, 552681 BD Biosciences), Siglec F PE (E50-2440, 552126 BD Biosciences), CD125 PE (T21, 558488 BD Biosciences), CD275 (HK5.3, 50598582 eBioscience), T1/ST2 FITC (1:100, DJ8, 101001F MD Bioproductos GmbH). Fc block (anti-CD16/CD32, 101302 Affymetrix) was included to minimize nonspecific antibody binding.

For T cell intracellular cytokine staining: anti-mouse IL-17A APC (TC11-18H10.1, 506916), IFN-ɣ BV421 (XMG1.2, 505830) and TNF-α FITC (MP6-XT22, 506 304) all from Biolegend.

Neutralizing antibodies: anti-IL-33 neutralising antibody (AF3626, Biotechne), anti-IL-5 (BE0198 BioXCell, TREK5), anti keyhole limpet hemocyanin isotype control (BE0090, BioXCell, LTF-2), anti-IFN-ɣR (BE0029, BioXCell, GR-20), anti-CCR3 (BE0316 clone 6S2-19-49), anti-horseradish peroxidase isotype control (BE0088, BioXCell, HRPN).

For high-dimensional spectral flow-cytometry analysis see Table S4.

For Western blotting membranes were probed with antibodies (1:1000) against vinculin (42H89L44, 700062 Thermo Fisher Scientific), phospho-p38 MAPK (Thr180/Tyr182, MA5-15218 Thermo Fisher Scientific) and phospho-p65 (Ser536, 93H1, 3033 Cell Signalling Technology).

For immunohistochemistry: rat anti-mouse SiglecF (E50-2440, 552126 BD Biosciences), Armenian hamster anti-mouse CD80 (16-10A1, 104729 Biolegend), rabbit anti-mouse p-NF-KB p65 (Ser536) (93H1,3033S Cell Signalling), mouse anti-human MBP (BMK-13, anti-human MBP (BMK-13, MCA5751 Bio-RAD), rabbit anti-human PD-L1 (E1L3N, 13684S Cell Signalling), mouse anti-EPX antibody (MM25-82.2.1, kindly provided by Dr. E.A. Jacobsen from Mayo Clinic, Scottsdale, AZ). Secondary antibodies (ThermoFisher): AlexaFluor goat-anti hamster 647, AlexaFluor goat anti-rat 594 (A-11007), AlexaFluor goat-anti hamster 647 (A-21451), AlexaFluor goat anti-rabbit 488 (A-11008), AlexaFluor goat anti-mouse 647 (A-21235).

Validation

All antibodies have been previously validated extensively by the manufacturer including by Western blot and confirmed by the authors for specificity and localization (no primary antibody control for IF and FMO for flow cytometry).

Animals and other organisms

Policy information about studies involving animals; ARRIVE guidelines recommended for reporting animal research

Laboratory animals

All experiments were performed on 6-16 week-old male and female mice. C57BL/6J (B6J, stock no. 000664), and dCas9-KRAB (stock no.030000) mice were obtained from The Jackson Laboratory; OT-1 (stock no. 003831), OT-II (stock no. 004194), MyD88-/- (Adachi et al, 1998), Tlr2-/- (stock no. 004650), CD45.1 (stock no.002014), Tlr4-/- mice (Hoshino et al, 1999) were obtained from a local live mouse repository. Id2CreERT2;Rosa26EYFP mice (Rawlins et al, 2019), Il5–transgenic mice (Dent et al, 1990) and Ifngr2fl/fl mice Lee et al, 2015) have been previously described. Il33−/− mice (Oboki et al, 2010) were obtained through the RIKEN Center for Developmental Biology (Acc.No.CDB0631K) and St2−/− mice have been described (Townsend et al, 2000) and backcrossed onto a C57BL/6J background. Eosinophil-deficient mice (PHIL, Lee et al, 2004) and mice expressing Cre under the EPX promoter (Eo-Cre, Doyle et al, 2013) were obtained from J.J. Lee (Mayo Clinic, Phoenix, AZ). Mice were maintained in a specific-pathogen-free (SPF) facility with a 12-h light-dark cycle, under controlled temperature (18-23°C) and humidity (40-60%), with ad libitum standard diet and water.

Wild animals

No wild animals were used in this study.

Field-collected samples

No field collected samples were used in this study.

Ethics oversight

All experimental procedures at the University of Zurich and Bern were performed in accordance with Swiss Federal regulations and approved by the Cantonal Veterinary Office and/or in accordance with the European Communities Council Directive (86/609/EEC),

Czech national guidelines, institutional guidelines of the Institute of Molecular Genetics and approved by the Animal Care Committee.

Note that full information on the approval of the study protocol must also be provided in the manuscript.

Flow Cytometry

Plots

Confirm that:

☒ The axis labels state the marker and fluorochrome used (e.g. CD4-FITC).

☒ The axis scales are clearly visible. Include numbers along axes only for bottom left plot of group (a 'group' is an analysis of identical markers).

☒ All plots are contour plots with outliers or pseudocolor plots.

☒ A numerical value for number of cells or percentage (with statistics) is provided.

Methodology

Sample preparation

Preparation of single-cell suspensions from tissues

Gastrointestinal tissues: stomach, colon and small intestine (SI) were harvested, cleaned of faecal matter and cut longitudinally. Organs were washed in PSB and cut into pieces (1-2cm) and Peyer's patches were removed from the SI. Pieces were washed twice in a shaking incubator with wash buffer (2% BSA, 100 U/mL penicillin/streptomycin, 5 mM EDTA in HBSS, 25 minutes, 37 °C). Tissues were then rinsed in cold PBS and digested for 50 minutes at 37°C in complete medium (10% FBS, 100 U/mL, penicillin/streptomycin (P0781 Sigma) in RPMI-1640) containing 15 mM Hepes (H0887 Sigma), 0.05 mg/mL DNase I (10104159001 Roche) and an equal amount of 250 U/mL type IV (C5138 Sigma) and type VIII collagenase (C2139 Sigma) (for colon and SI), or 500 U/mL type IV collagenase (C5138 Sigma) (for stomach). Cells were passed through a 70µm cell strainer, centrifuged for 8 minutes and layered onto a 40/80% Percoll (17089101 Cytiva) gradient (18 minutes, 2100 g, 20°C, no brake). The interphase was collected and washed in PBS.

Lung: lungs were perfused with PBS, harvested and cut into pieces before digestion in complete medium supplemented with 500 U/mL type IV collagenase (Sigma) and 0.05 mg/mL DNase I (Roche) for 50 minutes at 37°C. Lungs were then passed through a 70µm cell strainer and mesh with syringe plungers. To reduce macrophage contamination (Siglec F), cells were plated in complete RPMI medium for 1 hour at 37°C.

Blood: blood was sampled by post-mortem cardiac puncture in 2% BSA 5mM EDTA PBS. For Il5–tg mice, the suspension was layered over Histopaque 1119 (density of 1.119 g/mL; 11191 Sigma-Aldrich) and centrifuged at 800g for 20 minutes and the interphase was washed in PBS. Red blood cells were lysed in ice-cold distilled water for 30 seconds.

Bone marrow (BM): femur and tibia were flushed using complete RPMI medium and a 23-gauge needle. The content was collected, filtered through a 40µm cell strainer and red blood cells were lysed in ice-cold distilled water for 30 seconds.

Spleen, lymph nodes and thymus: spleen and lymph nodes were harvested, meshed through a 40µm cell strainer using a syringe plunger, and red blood cells were lysed in ice-cold distilled water for 30 seconds. Peritoneal fluid: peritoneal cavity was perfused with 5 mL PBS with a 21-gauge needle and the inflated area was massaged for 30 seconds, to disperse the solution. The peritoneal liquid was collected and cells were plated in complete RPMI medium for 1 hour at 37°C to remove adherent cells.

Adipose tissue: lungs were perfused with PBS and the perigonadal adipose depot was isolated, removing any visible gonadal tissue. The tissue was minced into small pieces and digested in complete DMEM medium supplemented with 0.2mg/mL Liberase (05401020001 Roche) and 0.05 mg/mL DNase I (Roche) for 50 minutes at 37°C. Suspensions were filtered through a 100µm cell strainer and centrifuged at 1000g for 10 minutes. The pellet was collected and washed in PBS.

Uterus: uterus was harvested, cut longitudinally and washed in PSB. Pieces were shaken in wash buffer (2% BSA, 100 U/mL penicillin/streptomycin, 5 mM EDTA in HBSS, 25 minutes, 37 °C). The tissue was then rinsed in cold PBS and digested for 50 minutes at 37°C in complete medium containing 0.05 mg/mL DNase I (Roche) and 0.2mg/mL Liberase (Roche). Cells were passed through a 70µm cell strainer, centrifuged and washed in PBS.

Unless specified, all centrifugation steps were performed at 500 g for 8 minutes at 10°C.

Staining: For surface staining, cells were stained in PBS at 4°C for 30 minutes with the fixable viability dye eFluor 780 (1:1000, 65-0865-14 eBioscience) and a combination of the following antibodies (1:200, all from BioLegend; unless stated otherwise): anti-mouse CD45 BV650 (30-F11, 103151), CD11b BV510 (M1/70, 101263), MHC-II AF700 (M5/114.15.2, 107622), Ly6G Percp-Cy5.5 (1A8, 127616), CD4 PerCP (RM4-5, 100538), TCRβ PE-Cy7 (H57-597, 109222), TCRβ PE-Cy7 (H57-597, 109228), CD80 BV605 (1:100, 16-10A1, 104729), PD-L1 PE-Cy7 (1:100, 10F.9G2, 124314), CD31 PE (390, 102408), CD45.2 BV785 (1:50, 104, 109839), CD9 PE (MZ3, 124805), CD54 BV711 (YN1/1.7.4, 116143), CD63 PE (1:100, NVG-2, 143904), CD95 PE-Cy7(SA367H8, 152607), SiglecE PE (M1304A01, 677104), Sca-1 AF488 (D7, 108116), Sca-1 AF700 (D7, 108142), C-kit BV605 (ACK2, 135121), CD11c APC-Cy7 (N418, 117323), Clec12a PE (5D3, 143404), CD49d FITC (R1-2, 103605), CD16/32 FITC (S17012B, 101305), CD3e Percp-Cy5.5 (145-2C11, 100328), CD8a APC (53-6.7, 100712), NK1.1 Percp-Cy5.5 (PK136, 108727), B220 Percp-Cy5.5 (RA3-6B2, 103236), Ter119 Percp (TER-119, 116227), Gr1 Percp (RB6-8C5, 108427), CD34 AF647 (RAM34, 560230), Siglec F BV421 (E50-2440, 552681 BD Biosciences), Siglec F PE (E50- 2440, 552126 BD Biosciences), CD125 PE (T21, 558488 BD Biosciences), CD275 (HK5.3, 50598582 eBioscience), T1/ST2 FITC (1:100, DJ8, 101001F MD Bioproductos GmbH). For T cell intracellular cytokine staining, cells were incubated for 3.15 hours in complete IMDM medium containing 0.1 µM

phorbol 12-myristate 13-acetate (P-8139 Sigma) and 1 µM ionomycin (I-0634 Sigma) with 1:1000 Brefeldin A (00-4506-51 eBioscience) and GolgiStop solutions (51-2092KZ BD Biosciences) in a humidified incubator with 5% CO2 at 37°C. Following surface staining, cells were fixed and permeabilized with the Cytofix/Cytoperm Fixation/Permeabilization Solution kit (512090KZ BD Biosciences) according to the manufacturer's instructions. Cells were then stained for 50 minutes with anti-mouse IL-17A APC (TC11-18H10.1, 506916), IFN-ɣ BV421 (XMG1.2, 505830) and TNF-α FITC (MP6- XT22, 506 304) all from Biolegend at 1:100. Fc block (anti-CD16/CD32, 101302 Affymetrix) was included to minimise nonspecific antibody binding. Total leukocyte counts were determined by adding countBright Absolute Counting Beads (C36950 Life Technologies) to each sample before analysis. Samples were acquired in a LSRII Fortessa or FACS AriaIII 5L (BD Biosciences). For high-dimensional spectral flow-cytometry analysis, cells were acquired on Cytek Aurora 5L (Cytek Biosciences) following 50 minutes staining at 4°C with the antibodies described in Table S3. For Click-iT Plus EdU Alexa Fluor 647 Flow Cytometry Assay Kit (C10419 ThermoScientific), the staining protocol was followed according to manufacturer's instructions. BD FACSDiva Software (BD Biosciences) was used for data acquisition and cell sorting.

Instrument	LSRII Fortessa or FACS AriaIII 5L (BD Biosciences), Cytek Aurora 5L (Cytek Biosciences)
Software	Aquired data were analyzed using FlowJo software.
Cell population abundance	Absolute numbers of cells are outlined in relevant Figures.
Gating strategy	Events were initially gated by FSC-A and SSC-A, then by FSC-A and FSC-H (to exclude doublets). Live CD45+ cells were then gated using a fixable viability dye. Subsequent gating depends on the population of interest and is outlined in Supplementary Information.

☒ Tick this box to confirm that a figure exemplifying the gating strategy is provided in the Supplementary Information.